Journal of Geochemical Exploration 177 (2017) 28–44

Contents lists available at ScienceDirect

Journal of Geochemical Exploration

journal homepage: www.elsevier.com/locate/gexplo

Light rare-earth element mineralization in hydrothermal veins related to the Jbel Boho alkaline igneous complex, AntiAtlas/Morocco: The role of fluid-carbonate interactions in the deposition of synchysite-(Ce)

Rachid Benaouda [a,b,*], Colin W. Devey [b], Lakhlifi Badra [c], Aomar Ennaciri [d]

[a] Institut für Geowissenschaften, Universität Kiel, 24118, Germany
[b] GEOMAR, Helmholtz Centre for Ocean Research, 24148 Kiel, Germany
[c] Faculté des sciences, Université My Ismail, Meknes, Morocco
[d] Managem Group, Marrakech, Morocco

ARTICLE INFO

Article history:
Received 1 June 2016
Revised 19 December 2016
Accepted 26 February 2017
Available online 1 March 2017

Keywords:
Synchysite
Rhabdophane
Hydrothermal
Quartz veins
REE mineralization
Jbel Boho

ABSTRACT

The world's largest mined rare-earth element deposits are associated with alkaline magmatism, making it important to understand the mechanisms leading to magmatic and hydrothermal element enrichment. We present results from late-differentiation-stage hydrothermal veins of the Jbel Boho alkaline complex in the district of Bou Azzer in the Anti-Atlas of Morocco, which show high light-REE enrichments. The REE mineralized veins occur around a syenitic pluton at the centre of the complex and consist of quartz-jasper and quartz veins which contain at least two silica generations. Only the second quartz generation is associated with LREE mineralization. The predominant REE-host mineral is the Ca-LREE-fluorcarbonate synchysite-(Ce), mainly present as anhedral crystals up to 200 μm. Some very small anhedral rhabdophane-(Ce) grains were also found in a synchysite-bearing quartz vein. Thermometric studies on mainly liquid-vapour-solid fluid inclusions in quartz crystals in the synchysite-bearing veins suggest very high salinity (32 to 37 wt% NaCl equiv.) of the mineralizing fluid. Homogenization temperatures from 150° to 250 °C provide the minimum temperature conditions in which the quartz veins were formed.

Based on recent experimental data, we propose a model for the formation of hydrothermal REE-Ca-F carbonate deposits in the veins, involving the transport of REE as chloride complexes at low pH conditions in the presence of fluoride ions. The deposition of synchysite is proposed to result from neutralization of this fluid by mixing of hydrothermal ore fluids with carbonate-rich meteoric water or by interaction with already existing carbonates in the vein, As well as raising the pH, this interaction also provides the Ca^{+} and CO_3^{2-} ions needed for REE precipitation as Ca-F carbonates.

The barren veins show two types of mineralogy and REE patterns: quartz-carbonate veins with enrichment of LREE over HREE and iron-rich jasper-bearing veins with quite flat REE pattern and high HREE. The LREE/HREE fractionation in these veins seems to be controlled by an interplay of two factors: 1) a low activity of ligands like Cl, which favours LREE transport and (2) the mineralogical control, by which HREE having similar ionic radii to Fe^{2+} will be preferred over LREE.

1. Introduction

Alkaline magmas, with their inherently high contents of mantle-incompatible elements, are good potential source rocks for rare-earth elements. For example the world's largest mined REE deposit, the Bayan Obo Fe-Nb-REE deposits in Inner Mongolia, China is related to hydrothermal activity in an alkaline igneous complex (Wu et al., 1996) and the Mountain Pass deposit in the USA is associated with carbonatite magmatism (Long et al., 2010). This provided evidence that these elements may be transported by magmatic and hydrothermal fluids and form valuable ore deposits (Smith et al., 2014, 2000; Smith and Henderson, 2000).

The increasing need for REE for the electronics industry and the present production from only a few localities worldwide (e.g., China with about 97% of the world REE production, Humphries (2013)) has led to an increase in prospection for alternative REE deposits.

Morocco possesses several alkaline complexes, of which the Tamazert complex (syenite-carbonatite) in the Central High Atlas is

* Corresponding author.
E-mail address: rbenaouda@geomar.de (R. Benaouda).

http://dx.doi.org/10.1016/j.gexplo.2017.02.002
0375-6742/

known for its association with REE minerals such as monazite, parisite and synchysite (Woolley, 2001). The Government's "Office National des Hydrocarbures et des Mines" (ONHYM) has additionally recently reported the occurrence of REE deposits with very high REE concentration (up to 3 wt%) linked with carbonatite rocks in the Ouled Dlim nappes of the Moroccan Mauritanides (ONHYM, 2015, 2013; Qalbi et al., 2011; Zerdane et al., 2011) in southern Morocco (Fig. 1).

The Jbel Boho alkaline complex was the subject of some works (Álvaro et al., 2006; Choubert, 1952; Ezzouhairi et al., 2008; Leblanc, 1981a), however no published study is available on the rare earth mineralization in this complex. Recently produced aeromagnetic studies on the Jbel Boho area (unpublished data from Managem mining company) show two strong magnetic anomalies, one related to the syenitic pluton and another further south, in an area overlain by the dolomitic cover (Fig. 2). The cause of the southern anomaly is unknown, although it may be related to another pluton. These anomalies led to preliminary mineral exploration work in this complex.

This study presents the first geochemical and petrological data on Jbel Boho REE mineralization as part of an integrated study that aims to identify the most REE-enriched rocks, the corresponding rare earth minerals and the origin of the ore-forming fluid responsible for the REE mineralization. This work reports for the first time the occurrence of the Ca-LREE-fluor-carbonate mineral synchysite ($REECa(CO_3)_2(F$-OH) as the main LREE host mineral and the rare REE-P mineral rhabdophane ($REEPO_4 \cdot nH_2O$) in late hydrothermal quartz veins of Jbel Boho, Förster (2001) and Augé et al. (2014) reported in detail the occurrence of synchysite in various rock types including magmatic (e.g. syenitic pegmatite, granite and carbonatite), metamorphic (e.g. metapelite and Apuan Alps metamorphic complex) and sedimentary rocks (carboniferous graywackes and karstic bauxite). In nature synchysite-(Ce) is the most abundant synchysite-group mineral, although synchysite-(Y) and rare synchysite-(Nd) also occur (Augé et al., 2014; Dawood et al., 2010; Förster, 2001; Maksimovic and Pantó, 1991). Some occurrences of synchysite were interpreted to be of primary origin (Smith et al., 2016; Uher et al., 2015; Zaitsev et al., 2014), however the generally accepted model for synchysite formation is by derivation from hydrothermal origin (Broom-Fendley et al., 2016; Doroshkevich et al., 2009; Förster, 2001, 2000; Förster et al., 2011; Gieré, 1996, 1990; Guastoni et al., 2009; Nadeau et al., 2015; Ngwenya, 1994; Ridolfi et al., 2006; Ruberti et al., 2008).

The work presented here shows clear evidences for synchysite formation in hydrothermal conditions. Most hydrothermal synchysite occurrences described in the literature indicate the formation of synchysite as replacement of pre-existing minerals. Consequently, synchysite mainly occurs associated with other REE-F carbonate minerals like bastnäsite and parisite. In Jbel Boho textural relationships

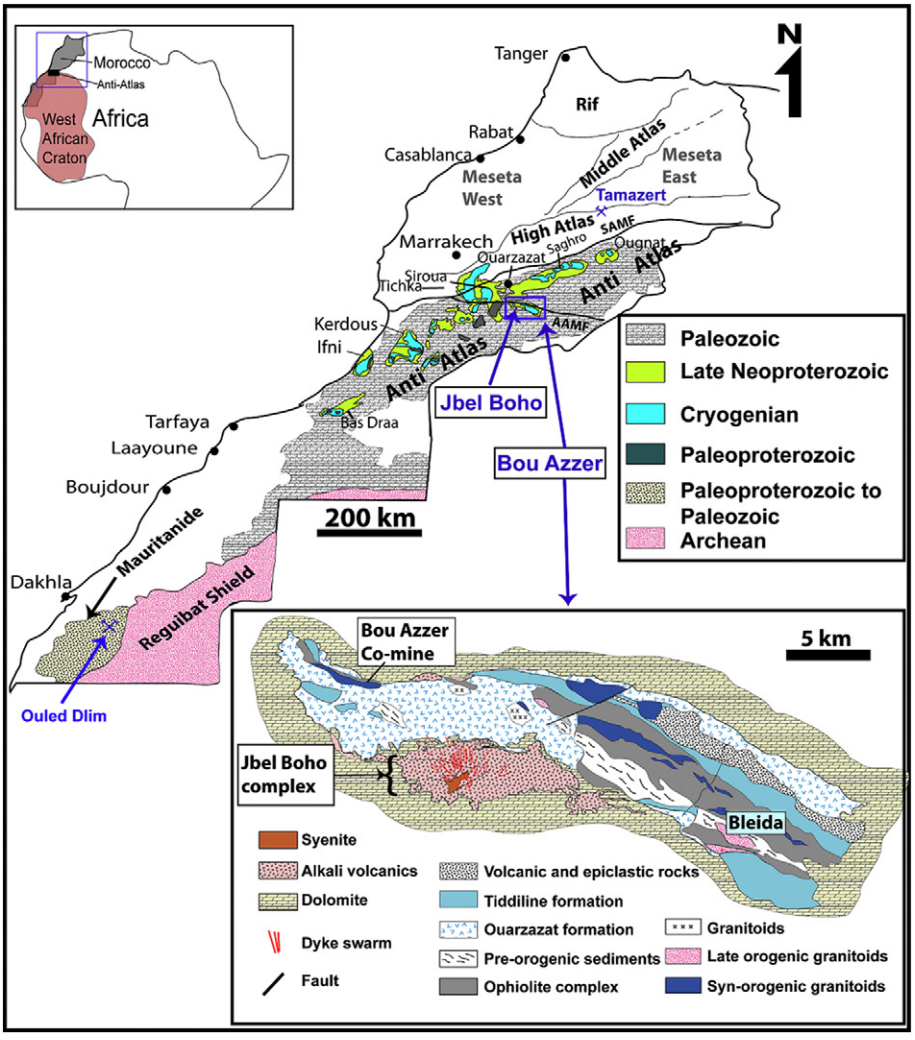

Fig. 1. A) Simplified geological map of Anti Atlas showing the location of the Bou Azzer inlier, modified after Guasquet et al. (2005). B) Simplified geological map of Bou Azzer showing the location of Jbel Boho complex, modified after Leblanc (1981a). SAMF (South Atlas Major Fault) and AAMF (Anti-Atlas Major Fault).

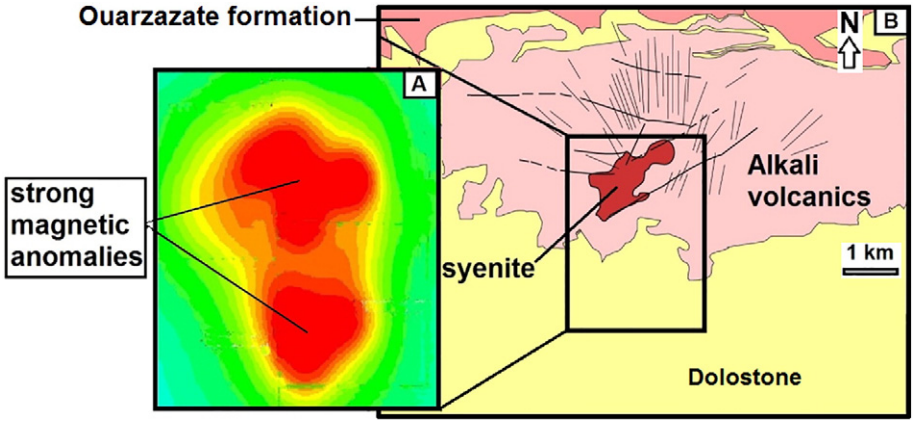

Fig. 2. A) Magnetic anomaly map (Managem internal document) showing two strong anomalies around the syenitic intrusion and the dolostone. The approximate position lies between Long: −6.789; Lat: 30.433 and Long: −6.821; Lat: 30.394. B) geological map of Jbel Boho modified after Leblanc (1981a).

clearly shows isolated synchysites within quartz veins suggesting a direct precipitation from the fluid.

2. Geological setting

The Bou Azzer inlier is a productive mining area, known in particular for the cobalt-arsenide deposits in the Bou Azzer mine, the copper deposit at Bleida and gold-palladium deposits at Bleida Far West related to the Bou Azzer ophiolite (Belkabir et al., 2008; El Ghorfi et al., 2008; Ennaciri et al., 1995; Leblanc, 1981b, 1972; Oberthür et al., 2009).

The Jbel Boho alkaline complex consists of a lava series intruded by a polyphase syenite complex and then finally by a dyke swarm. It is the best-preserved igneous complex in the south-western part of the Bou Azzer inlier in the Anti-Atlas (Fig. 1). All Jbel Boho rocks are cross cut by quartz-carbonate veins with different forms and mineral assemblages (mainly quartz, jasper and carbonate). The main mineralized hydrothermal veins crop out north of the syenite pluton along a fault zone, with an orientation of roughly N50°E.

Zircon U-Pb geochronological studies on a syenite (534 ± 10 Ma) and a trachyte (from the locality Aghbar, 531 ± 5 Ma) from Jbel Boho show the complex to be Early Cambrian in age (Ducrot and Lancelot, 1977; Gasquet et al., 2005). It was emplaced on the northern edge of the West African Craton (WAC). It represents a late magmatic event in the Pan-African evolution of the region, which was itself marked by two tectonic regimes: a compressive regime, which resulted in the emplacement of the ophiolite (ca 760–700 Ma) comprising much of the core of the Bou Azzer inlier, and a later extensional regime represented by calc-alkaline magmatism of the Ouarzazate Group (ca 545–580 Ma) and the early Cambrian alkaline magmatism of the Jbel Boho complex (Gasquet et al., 2008, 2005).

The lava flows associated with Jbel Boho magmatism are intercalated with dolostones (from the lower Adoudounian formation) and overlapped by the upper Adoudounian dolostone and lie-de-vin series. According to several authors (Algouti et al., 2001; Álvaro et al., 2006; Piqué et al., 1999; Soulaimani et al., 2003) normal faulting accompanied by an extensional tectonic regime related to rifting led to the alkaline magmatism of Jbel Boho and simultaneously to the deposition of the Adoudounian carbonate. Although no pillow-lavas are seen, the association with dolostones suggests submarine volcanic activity in sub-aerial to shallow water conditions.

The Jbel Boho complex was produced from at least three generations of magma (Benaouda, 2015): an initial magmatic event generated alkaline lava flows showing a strong enrichment of the LREE relative to the HREE and strong negative Eu anomalies; a subsequent magma batch produced the polyphase syenitic intrusion (Fig. 1) consisting of olivine syenite and quartz syenite which display REE patterns and trace element anomalies different to those of the lavas; the third magmatic event produced microsyenitic and subalkaline rhyolitic dykes with different high field-strength element HFSE signatures to the other rocks.

3. Samples and methodology

Samples of quartz-carbonate veins were collected systematically along a broad northeast-southwest transect across the complex (Fig. 3). After macroscopic and microscopic examination, 21 samples were selected for chemical analysis. Whole rock analyses of major- and trace elements were performed at the ACME Analytical Laboratories Ltd., Vancouver (Canada) using X-ray fluorescence (XRF) and laser ablation inductively coupled plasma mass spectrometer (LA-ICP-MS) techniques. Major element detection limits range from 0.01 to 0.1 wt% and trace element detection limits range from 0.01 to 1 ppm, except the values of gold (Au), which are given in ppb with detection limit of 0.5 ppb. The compositions of minerals were determined using a JEOL JXA 8900R electron microprobe at the Institute of Geosciences, University of Kiel, Germany. The composition of fluid inclusions was determined using a Linkam THM 600 heating/cooling stage attached to an Olympus microscope. This allows microthermometry to be performed on the fluid inclusions over the temperature range 600 °C to −196 °C. Temperature calibration was carried out using a set of synthetic inclusions distributed by Fluid Inc., USA, in the temperature range of −56.6 °C to 0.0 °C. The precision of the temperature measurements was about ±0.2 °C in a temperature range of −60 to +100 °C, within ±0.5–2 °C in the range of −60 to −120 °C, within ±3 °C from −120 °C to −140 °C and about ±2 °C for temperatures above 100 °C.

4. Petrography and geochemistry of the late hydrothermal veins

4.1. Petrography

Variously orientated hydrothermal quartz-carbonate veins occur in all rock types of the Jbel Boho alkaline complex (Fig. 4 and Fig. 5), displaying thicknesses between 20 cm and 2 m. They crop out over a distance of a few metres to several tens of metres on the surface. The hydrothermal veins are mainly quartz dominated with variable contents of dolomites and calcites as well as jasper, an opaque, Fe-rich variety of jasper-chalcedony. Jasper occurs only around the quartz syenite.

We subdivided the veins based on the presence of synchysite into two categories, namely the REE mineralized veins (group 1, G1) and

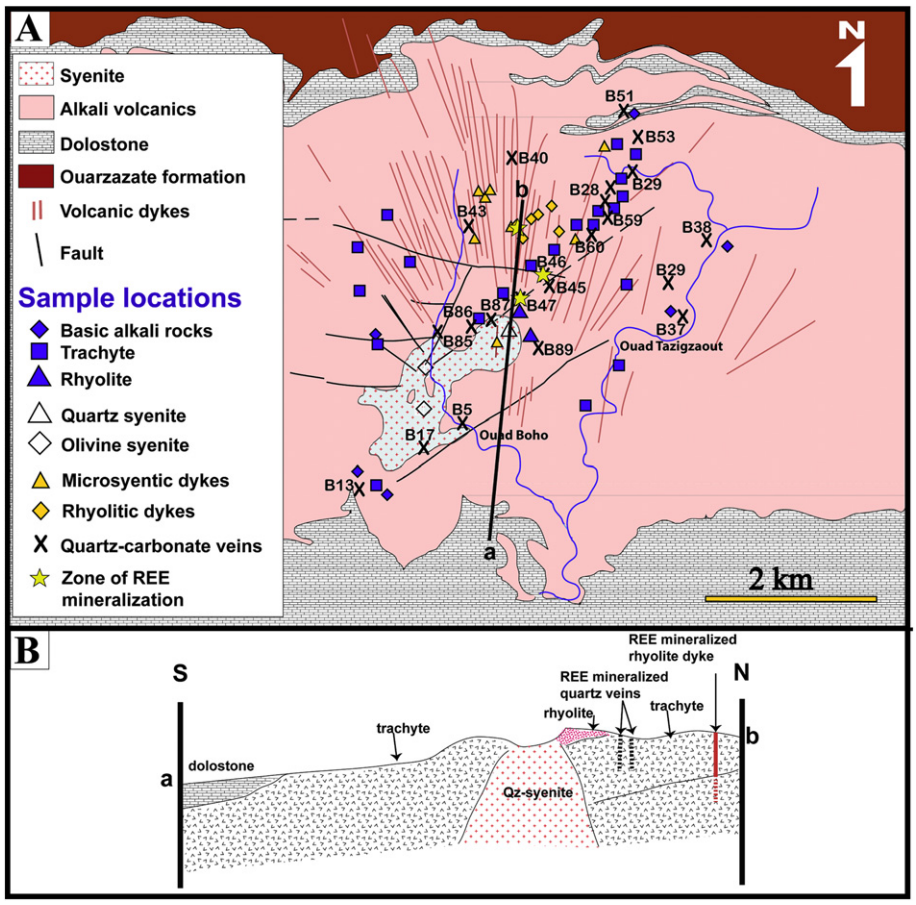

Fig. 3. A) Geological map of Jbel Boho complex modified after Leblanc (1981a), showing the sampling locations. B) N-E cross-section showing the locations of the REE mineralized zones north of the quartz syenite.

barren veins. As the barren veins show two distinct REE-patterns (steep and flat patterns) they are subdivided into two groups (G2 with steep REE-patterns and G3 with flat REE-patterns; see Section 4.2).

4.1.1. The REE mineralized veins

The main REE mineralized veins (Fig. 3A–B; Table 1 G1) consist of a quartz vein (sample B46-3; Fig. 5A) and quartz-jasper vein (B47, Fig. 5B, C and D) that are oriented N50°E along a subvertical fault zone and show thicknesses up to ~1.5 m. The other veins of the G1 group have low synchysite contents, which are optically very difficult to identify.

The presence of slickensides on the footwall of the quartz-jasper vein indicates that the fault continued to move after the formation of the vein (Fig. 5E). The fault plane and the direction of the slickenlines, which indicate a slip vector of 25° to the SW relative to the fault strike (N50°E), indicates an oblique dextral strike-slip fault.

The quartz-jasper vein is composed of jasper (dense and opaque microcrystalline quartz that is of red-brownish colour due to Fe- and Mn-Fe oxides), which is itself cut by later quartz veins (Fig. 5B) that contain small synchysites (up to 100 μm). Synchysites occur both as inclusions in quartz crystals and in equilibrium with them (Fig. 6A). Rhombs of dolomite occur between the synchysite-bearing quartz and the jasper (Fig. 6B). The dolomites show leached zones in the rhombs resulting from the replacement of carbonate with Mn- and Fe-oxides. Synchysite is the only REE-host mineral in the LREE-enriched quartz-jasper vein.

The REE mineralized quartz vein (B46-3) is composed of zoned and coarse-grained quartz crystals (1 mm to 3 mm in size) cross-cut by fine grained quartzes (up to 250 μm) that contain synchysite minerals with very similar petrographic relationships to those seen in the quartz-jasper vein. The mineralized quartz vein contains two REE-host minerals, synchysite (the main REE-host mineral) and occasionally tiny rhabdophane crystals.

Under the polarizing microscope the synchysite crystals in both types of REE mineralized veins appear colourless to slightly yellow with high relief. They form subhedral to euhedral crystals (Fig. 6A and C), which display sometimes very good idiomorphic form as illustrated in a thick section micrograph (Fig. 6D).

4.1.2. The barren veins

The barren veins (G2, G3; Tables 2, 3) occur in all Jbel Boho rock types. They consist of quartz-carbonate (dolomite and calcite) veins with dominance of quartz in most veins.

The lower dolostones are also cut by small quartz veins, in which euhedral dolomite rhombs (generally from 10 to 400 μm in size), anhedral calcite and occasionally chabazite ($Ca(Al_2Si_2O_{12})\cdot 6H_20$) crystals occur (Fig. 7A). The carbonate rhombs show strong dissolution of the core and part of the rim or vice versa.

The quartz crystals in the hydrothermal veins within the magmatic rocks are anhedral to subhedral with varying grain sizes from 0.1 to 3 mm (Fig. 7B). The dolomite rhombohedrons occur within quartz as isolated euhedral crystals or subhedral aggregates with sizes mostly in the

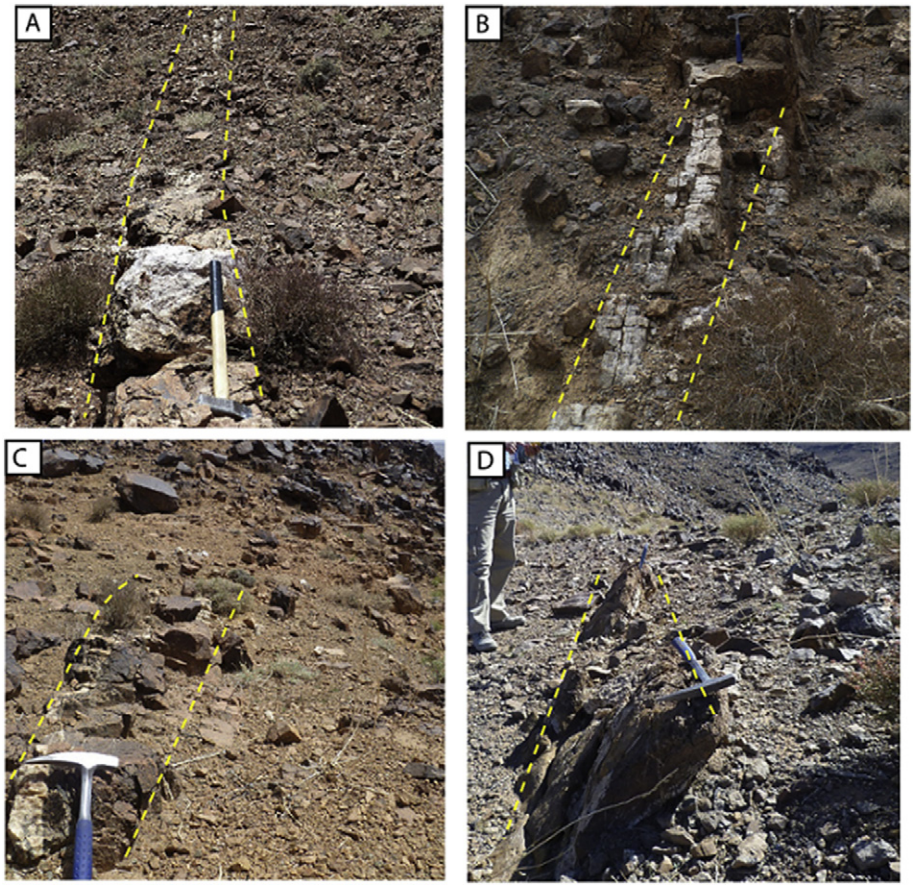

Fig. 4. Examples of hydrothermal ore-barren veins with low REE contents: A) quartz vein cutting trachyte, B) quartz vein cutting phonotephrite, C) quartz-jasper vein in trachyte near syenite, D) carbonate-dominated vein in trachyte.

range from 0.1 mm to 0.7 mm. Zonation within individual dolomite crystals is reflected by either clear core or cloudy rims or vice versa. Microprobe examination shows that the dark and light zones in the dolomite rhombs correspond to Mg rich- and Ca-rich carbonate zones respectively (Fig. 7C). Muscovite occurs occasionally as small colourless inclusions in some quartz veins with grain sizes up to 0.1 mm (Fig. 7D). Some quartz veins near to the syenite show quartz crystals with euhedral zoning. The zonation can be easily observed under a polarization microscope (Fig. 7E) especially for quartz crystals with sizes over 1 mm. With decreasing crystal sizes, the growth zones become less evident.

Some jasper-bearing barren veins are mainly found adjacent to the quartz syenite. They are the least abundant of all veins and have a preferred orientation from N20°E to N50°E similar to the orientation of the REE mineralized veins, but with thickness generally <30 cm. In thin section, the microcrystalline quartz in the jasper is fibrous and so is classified as chalcedony (Fig. 7F).

4.2. Geochemistry

The REE patterns of all vein samples plotted relative to C1-chondrite (McDonough and Sun, 1995) are shown in Fig. 8. All veins show negative Eu anomalies (Fig. 8A, B and C). A sample (B51-1) from the lower dolostones, which are intercalated with the volcanic rocks, is added to Fig. 8D for comparison. It shows higher LREE contents than either groups G2 or G3 and also a slight enrichment of the LREE relative to the HREE, but without any Eu anomaly. The REE pattern of the lower dolostone is very similar to that of the basic volcanic rocks (dashed line, Fig. 8D).

The group G1 veins (see also Table 1) shows strong LREE enrichment relative to the HREE. They have all very similar LREE patterns with somewhat more variable HREE, and ΣREE contents between 1505 and 292 ppm. It is important to note that the veins of the group G1 all occur directly adjacent to the syenite and show similar NE-SW directions and that some veins even cut the syenitic pluton, whereas the veins of the groups G2 and G3 occur elsewhere within the volcanic rocks.

The group G2 (Table 2) has similar HREE patterns to G1 but with much lower LREE concentrations. The ΣREE content ranges from 154 to 18 ppm, with no specific REE minerals identifiable.

The group G3 (Table 3) shows, unlike the two other groups, very flat REE patterns with a peak in the middle REE (Gd, Tb and Dy) and ΣREE contents ranging between 87 and 223 ppm. They show the highest HREE contents of all vein types. The G3 group consists of carbonate-dominated veins, which show generally higher iron contents than the other veins, with Fe_2O_3 ranging from 3.5 to 7.8 wt%.

5. Composition of the observed accessory rare earth minerals

The REE-host minerals responsible for the high LREE enrichment in the G1 veins were subject to microprobe chemical analysis. The results of the chemical analysis for these minerals are summarized in Table 4 and Table 5 and described below.

5.1. Synchysite-(Ce)

Synchysite is a member of the REE-fluorcarbonate mineral group, whose principal mineral bastnäsite is the main REE ore mineral in

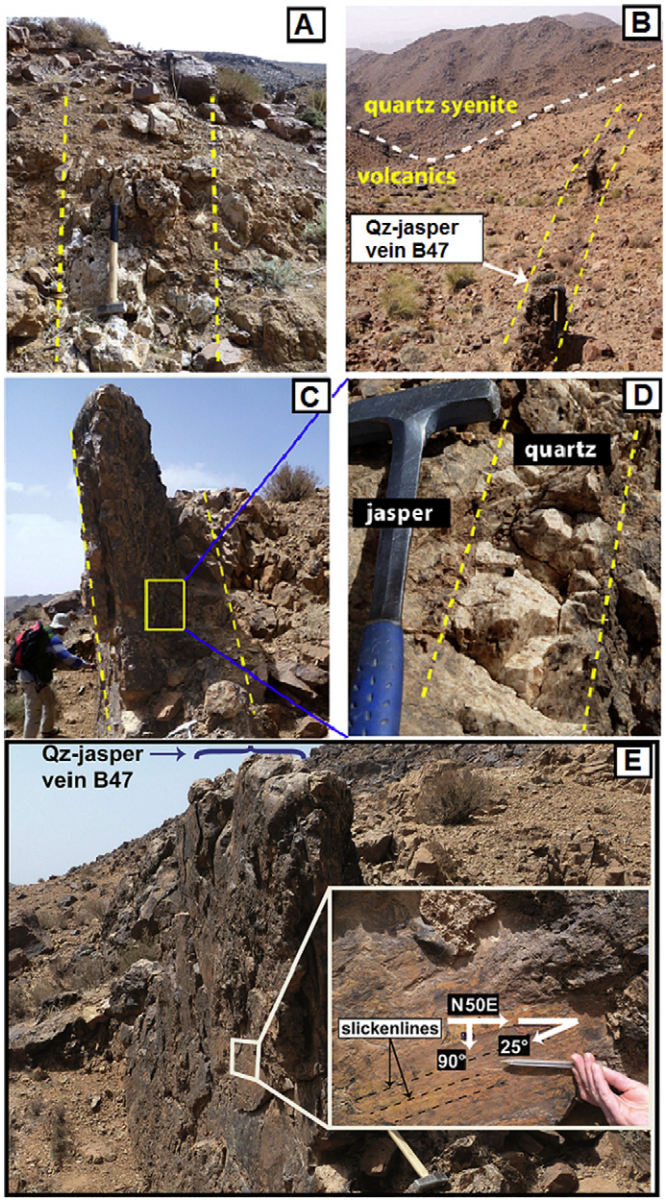

Fig. 5. Examples of synchysite-bearing veins with high REE contents: A) synchysite- and rhabdophane-bearing quartz vein (B46) in trachyte, B) large synchysite-bearing quartz-jasper vein next to syenite (B47) cutting the neighbouring volcanics, C) and D) the same vein (B47) showing quartz veins within jasper, E) structural characteristic of the fault hosting LREE enriched quartz-jasper vein, which occurs in the footwall of the fault. The orientation of the slickenlines indicates an oblique dextral strike-slip movement.

Table 1
Major (wt%) and trace elements (ppm) contents of Jbel Boho hydrothermal veins (G1 group).

G1 veins							
	B46–3	B47–7	B46–2	B17–1	B13–2	B5–1	B86
SiO_2	97.30	97.80	98.40	91.50	78.70	95.60	98.40
TiO_2	0.15	0.08	0.06	<0.01	<0.01	<0.01	0.01
Al_2O_3	1.04	0.22	0.73	0.58	0.70	0.32	0.20
Fe_2O_3	0.29	0.42	0.28	1.90	0.75	0.42	0.59
MnO	0.02	0.05	0.03	0.07	0.10	0.05	<0.01
MgO	0.08	<0.01	0.06	0.05	3.62	0.05	0.01
CaO	0.15	0.05	0.15	2.84	5.83	1.37	0.05
Na_2O	0.03	0.05	0.07	<0.01	0.01	<0.01	0.07
K_2O	0.32	0.07	0.23	0.09	0.10	0.03	0.06
P_2O_5	0.06	<0.01	0.02	0.03	0.05	0.02	<0.01
Cr_2O_3	<0.001	<0.001	<0.001	<0.001	<0.001	<0.001	<0.001
LOI	0.53	0.37	0.47	2.74	9.02	1.35	0.42
Total	99.97	99.11	100.50	99.80	98.88	99.21	99.81
Ba	33.00	37.00	21.00	116.00	77.00	17.00	28.00
Rb	8.20	2.80	5.50	2.70	4.10	0.90	2.60
Sr	16.9	13.0	8.7	21.3	95.7	17.2	21.3
Zr	29.8	45.7	9.50	11.2	6.90	1.50	4.90
Nb	7.30	6.40	2.20	1.10	1.00	0.80	2.70
Ni	0.50	0.80	0.30	1.40	0.20	0.80	0.50
Co	0.80	2.90	0.20	2.10	0.60	0.90	0.70
Zn	5.00	5.00	2.00	18.0	2.00	2.00	6.00
La	336	224	122	88.1	120	76.1	66.6
Ce	712	423	263	201	174	170	150
Pr	74.19	47.59	28.77	23.94	16.44	20.39	13.65
Nd	287	169	107	90.0	51.6	74.0	44.9
Sm	41.77	25.24	15.23	16.39	7.41	13.58	6.68
Eu	5.44	3.05	1.96	2.68	0.98	1.97	0.85
Gd	25.72	17.35	8.40	10.47	4.57	8.20	4.18
Tb	1.96	1.46	0.67	0.94	0.53	0.59	0.31
Dy	5.02	5.03	1.99	3.09	2.04	1.53	0.99
Y	14.6	19.5	4.80	8.40	6.70	2.80	3.10
Ho	0.28	0.53	0.09	0.34	0.27	0.09	0.07
Er	0.51	0.91	0.05	0.74	0.56	0.14	0.12
Tm	0.06	0.15	0.04	0.10	0.06	0.02	0.02
Yb	0.64	1.03	0.26	0.71	0.41	0.17	0.06
Lu	0.07	0.11	0.02	0.10	0.05	0.02	0.02
ΣREE	1504.96	937.15	553.58	447.20	385.42	369.80	291.65
Ta	0.40	0.50	0.20	<0.10	<0.10	0.10	<0.10
Hf	1.00	1.00	0.30	<0.10	<0.10	<0.10	0.10
As	<0.50	3.10	0.80	31.70	<0.50	1.60	<0.50
Ag	<0.10	<0.10	<0.10	<0.10	<0.10	<0.10	<0.10
Au	1.50	<0.50	1.80	<0.50	0.90	0.70	14.80
Ga	2.90	1.00	2.30	1.70	1.60	0.70	<0.50
Mo	1.20	2.40	0.40	7.00	0.40	1.00	0.90
Cu	30.3	9.90	23.1	66.4	11.7	40.9	605
Pb	1.40	2.00	0.60	4.50	0.50	1.10	2.50
Th	2.60	8.70	2.40	0.70	0.20	<0.2	0.30
U	0.50	0.50	0.10	0.10	0.10	<0.10	0.20
Cs	0.20	0.10	0.10	0.10	0.20	<0.10	0.40
V	15.00	<8.00	12.00	<8.00	<8.00	<8.00	<8.00

the world. The atomic arrangement of synchysite was described by Ni et al. (1993) and Wang et al. (1994) who, based on 3D X-ray-diffraction data, suggested a layered structure, with bastnäsite (CeF) and (Ca) layers separated by layers of carbonate groups (CO_3^{2-}). Considering the ratios of (CeF):(CO_3):($CaCO_3$) layers, the synchysite can be cast as 1:1:1 whereas bastnäsite is 1:1:0. Unlike the hexagonal symmetry of bastnäsite, these authors show that the true symmetry of synchysite is monoclinic, which confirms the predictions of Donnay and Donnay (1953). The OH^- content in synchysite was, however, not reported in these works. Guastoni et al. (2009) determined the OH content in synchysite experimentally, concluding that it well matched to the amount F which appeared to be messing in the calculated chemical formula ($F_{0.643}$) of Wang et al. (1994). These authors concluded that synchysite contained 0.643 atoms per formula unit (pfu) although the stoichiometry would imply that 1 atom of F pfu should be present. The quantity of 0.357 OH pfu in synchysite determined by Guastoni et al. (2009) apparently substitute for F.

Table 4 summarizes the synchysite compositions in the LREE enriched quartz veins (this study) and the rhyolitic dyke B35 (Benaouda, 2015). The CO_2 values in wt% are calculated to arrive at analytical total of 100 wt%. All analysed minerals in this study have Ce as the dominant cation and may therefore be termed synchysite-(Ce). All synchysites are enriched in the LREE, especially La, Ce and Nd. The La_2O_3 values range from 11.65 to 14.46 wt%, Ce_2O_3 from 19.78 to 22.48 wt% and Nd_2O_3 from 9.25 to 10.85 wt%. Thorium is very low in synchysite-(Ce), generally <0.04 wt%. The calculated formula (ΣREE + Th: 0.98, Ca: 1.04, F: 0.74, C: 2.14) is

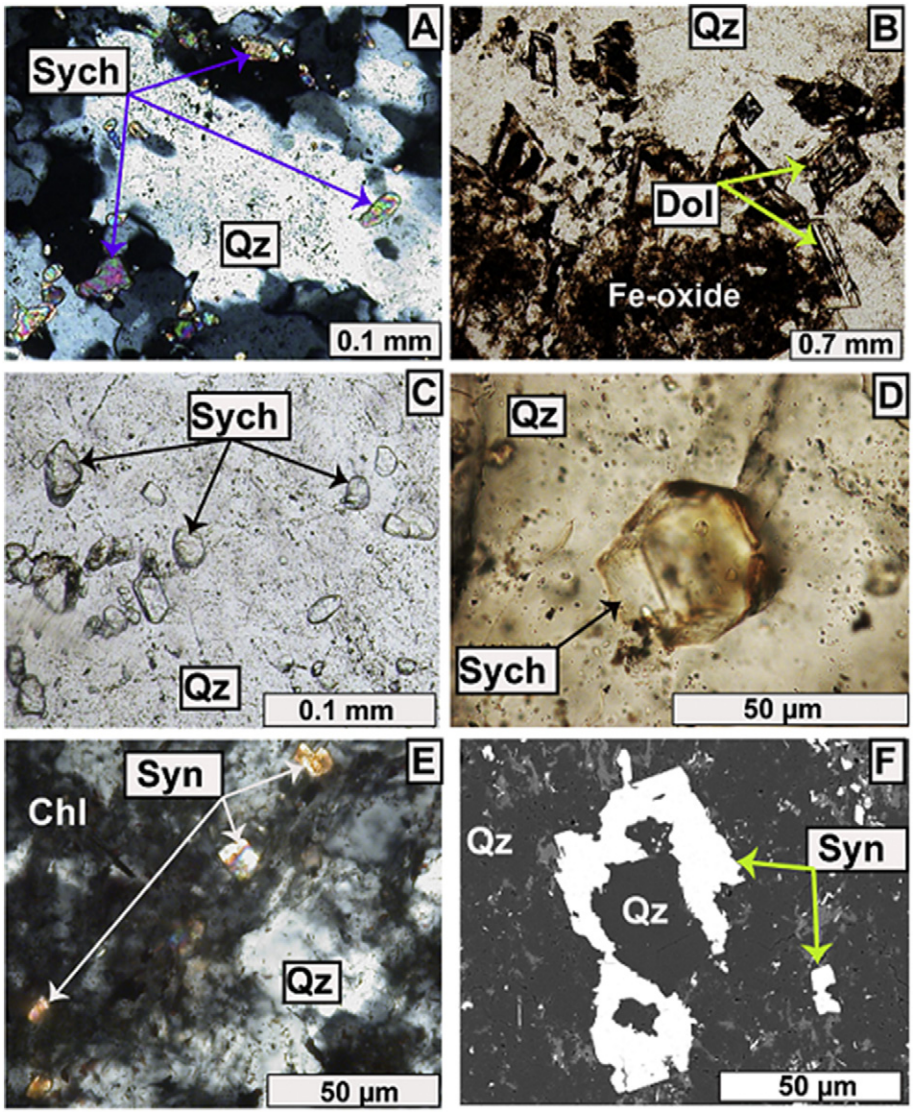

Fig. 6. Photomicrographs showing the occurrence of synchysite and carbonate in the REE mineralized veins: A) association of synchysite with quartz crystals in the quartz-jasper vein (B47), B) altered dolomitic rhombs between quartz and jasper, C) synchysite grains within quartz in the quartz vein (B46-3), D) idiomorphic synchysite in a thick section from (B46-3), E) and F) show synchysite occurrences within a rhyolitic dyke.

consistent with the synchysite composition with an F pfu deficit of ~0.26 due to OH substitution (Guastoni et al., 2009) as discussed above.

The C1-chondrite normalized REE of synchysite-(Ce) minerals from the two quartz veins B47 and B46-3 and rhyolitic dyke B35 are presented in Fig. 9A–C. The synchysites are strongly enriched in LREE. The grey field represents the REE distribution patterns of both analysed REE minerals (synchysite and rhabdophane). Their REE patterns decline from La to Gd with slight to strong negative Eu anomalies. The HREE contents are, with the exception of Y, generally below the detection limits.

5.2. Rhabdophane-(Ce)

The REE-P mineral rhabdophane is a hydrated phosphate of REE with mineral chemistry similar to monazite $XPO_4.nH_2O$ [X: REE, Ca, Th, U and n: number of water molecules]. Unlike monazite, which is monoclinic, the crystal structure of rhabdophane is hexagonal (Mooney, 1950) with a postulated H_2O content (n) between 0.5 and 1.5. Thermal reactions of rhabdophane led to the water corresponding to nH_2O being considered as zeolitic water (Hikichi et al., 1996, 1988, 1978). This water is incorporated as non-stoichiometric molecules in large channels along the c-axes in the hexagonal structure of rhabdophane (Kijkowska et al., 2003).

Rhabdophane is found only in the LREE-rich quartz vein B46-3 as small isolated grains with sizes up to 20 µm. The analysed rhabdophane minerals contain abundant LREE, notably Ce, La and Nd while the proportion of the HREE is very low. The results are summarized in Table 5 and show Ce_2O_3 content ranging between 23.7 and 31.3 wt%, La_2O_3 content between 14 and 16 wt% and Nd_2O_3 between 11.5 and 13.5 wt%. The Pr_2O_3 content is about 3.3 wt% and Sm_2O_3 is about 1.8 wt%. Of the HREE, only two elements were detected in minor amounts (Gd_2O_3 ~ 1 wt% and Y_2O_3 ~ 0.2 wt%). All other REE are under the detection limit for EPMA. Like synchysite-(Ce), rhabdophane shows a predominance of Ce over all other REE, classifying this REE mineral as rhabdophane-(Ce). Unlike monazite, the CaO content is significant with an average of 2.7 wt% and the ThO_2 content is very low with an average of 0.05 wt%.

Table 2
Major (wt%) and trace elements (ppm) contents of Jbel Boho hydrothermal veins (G2 group).

G2 veins							
	B40–4	B87	B46–1	B37	B40–1	B28–1	B38
SiO_2	95.40	97.40	97.20	96.10	98.20	82.40	98.70
TiO_2	0.06	<0.01	0.14	<0.01	<0.01	0.09	<0.01
Al_2O_3	1.30	0.23	1.00	0.86	0.45	6.48	0.24
Fe_2O_3	0.33	0.82	0.36	0.22	0.16	1.37	0.04
MnO	0.03	<0.01	0.02	0.02	0.03	0.04	<0.01
MgO	0.08	<0.01	0.08	0.22	0.02	0.27	<0.01
CaO	0.29	0.05	0.05	0.50	0.23	1.84	0.16
Na_2O	0.02	0.07	0.09	<0.01	0.04	0.05	<0.01
K_2O	0.35	0.05	0.51	0.20	0.11	3.27	0.02
P_2O_5	0.02	<0.01	0.01	<0.01	<0.01	0.04	<0.01
Cr_2O_3	<0.001	<0.001	<0.001	<0.001	<0.001	0.00	<0.001
LOI	0.77	0.81	0.49	0.99	0.55	2.52	0.31
Total	98.65	99.43	99.95	99.11	99.79	98.37	99.47
Ba	159	27	52	50	56	2760	8
Rb	10.1	2.0	11.7	7.30	1.70	86.7	0.60
Sr	42.6	27.1	17.0	14.2	8.10	67.2	9.10
Zr	41.7	5.1	36.3	7.80	7.00	60.9	1.30
Nb	8.20	2.00	5.50	1.20	1.30	3.30	0.40
Ni	1.40	0.80	0.50	0.50	0.40	0.80	0.10
Co	0.90	1.00	0.40	0.40	0.40	0.60	0.60
Zn	3.00	8.00	7.00	3.00	2.00	2.00	<1
La	36.1	17.3	12.8	14.2	7.10	3.50	3.60
Ce	63.2	35.0	26.3	21.1	13.2	6.60	8.50
Pr	7.26	3.68	3.08	2.11	1.67	0.93	0.96
Nd	27.7	12.0	11.4	7.80	8.00	3.70	3.50
Sm	4.82	1.84	1.82	1.27	1.29	1.07	0.51
Eu	0.65	0.26	0.26	0.29	0.22	0.30	0.09
Gd	3.20	1.18	1.53	2.08	0.98	1.37	0.38
Tb	0.39	0.12	0.16	0.36	0.11	0.21	0.03
Dy	1.70	0.60	0.62	1.99	0.44	1.27	0.09
Y	7.50	2.00	3.30	8.60	1.80	8.00	0.40
Ho	0.26	0.05	0.13	0.27	0.08	0.31	0.02
Er	0.59	0.13	0.37	0.55	0.10	0.89	0.04
Tm	0.09	0.02	0.05	0.06	0.03	0.13	0.01
Yb	0.71	0.05	0.46	0.32	0.14	0.89	0.05
Lu	0.07	0.01	0.04	0.04	0.03	0.13	0.01
ΣREE	154.24	74.24	62.32	61.04	35.19	29.30	18.19
Ta	0.50	0.10	0.30	<0.10	<0.10	0.30	<0.10
Hf	1.00	0.20	0.80	0.20	0.10	1.60	<0.10
As	4.30	<0.50	1.00	0.60	1.30	<0.50	<0.50
Ag	<0.10	<0.10	<0.10	<0.10	<0.10	<0.10	<0.10
Au	<0.50	<0.50	<0.50	2.20	1.40	<0.50	<0.50
Ga	3.50	<0.50	2.60	1.70	3.10	6.00	2.10
Mo	0.60	<0.10	0.70	0.30	0.20	0.50	<0.10
Cu	7.50	4933	6.80	19.60	25.10	1.10	14.70
Pb	1.00	2.30	1.40	1.00	1.20	1.10	1.30
Th	1.50	0.20	1.10	0.20	0.20	2.70	<0.2
U	0.50	<0.10	0.40	0.10	0.10	0.60	<0.10
Cs	0.20	0.50	0.30	0.30	<0.10	1.70	0.10
V	25.00	<8.00	16.00	<8.00	<8.00	13.00	<8.00

Table 3
Major (wt%) and trace elements (ppm) contents of Jbel Boho hydrothermal veins (G3 group).

G3 veins							
	B29	B89	B59–1	B-60	B43	B85–4	B51–1
SiO_2	4.20	88.90	89.60	17.10	14.30	94.00	51.00
TiO_2	0.04	0.03	0.03	<0.01	0.10	<0.01	0.41
Al_2O_3	0.28	0.39	0.40	0.11	0.88	0.22	11.87
Fe_2O_3	3.49	6.63	5.82	4.33	7.78	3.69	4.87
MnO	0.78	1.10	0.91	0.82	1.20	0.43	0.32
MgO	1.22	0.07	0.10	11.50	0.64	0.03	0.51
CaO	49.39	0.25	0.18	30.30	40.95	0.14	13.70
Na_2O	<0.01	<0.01	<0.01	<0.01	0.03	<0.01	6.22
K_2O	0.02	0.10	0.12	0.01	0.11	0.05	0.68
P_2O_5	0.01	0.03	0.02	<0.01	0.02	0.01	0.11
Cr_2O_3	0.00	<0.001	<0.001	<0.001	0.00	<0.001	<0.001
LOI	40.34	2.42	2.35	34.59	33.99	1.65	9.55
Total	99.77	99.92	99.53	98.76	100.00	100.22	99.24
Ba	909	1224	1332	551	13	229	115
Rb	3.00	3.70	4.40	0.50	7.20	1.00	18.0
Sr	76.2	27.3	18.3	39.2	129	21.9	142
Zr	4.50	11.7	11.3	1.60	7.10	3.90	398
Nb	1.20	2.10	1.90	0.40	1.70	0.80	75.50
Ni	<0.10	3.80	3.40	2.30	<0.10	0.40	0.70
Co	1.50	4.30	4.10	2.50	4.10	0.90	2.30
Zn	3.00	32.0	47.0	2.00	4.00	3.00	18.0
La	9.40	23.3	5.60	4.30	9.20	13.8	50.6
Ce	25.8	44.4	10.5	12.7	18.1	18.0	107
Pr	4.09	6.11	2.12	2.00	2.27	3.25	13.26
Nd	22.4	25.0	11.4	9.70	10.5	14.6	53.5
Sm	9.53	8.02	4.63	4.94	3.23	3.47	10.90
Eu	2.43	1.74	1.08	0.99	0.78	0.77	3.13
Gd	16.25	11.74	8.51	8.39	5.07	4.80	9.85
Tb	3.51	2.26	2.04	2.22	1.12	0.92	1.39
Dy	19.4	11.1	12.4	13.5	6.45	4.86	8.20
Y	90.9	36.4	55.9	50.6	26.0	18.5	40.4
Ho	3.35	1.67	2.04	2.16	0.99	0.74	1.42
Er	7.80	3.49	4.88	5.40	1.93	1.66	4.03
Tm	1.05	0.40	0.63	0.75	0.29	0.20	0.63
Yb	6.62	2.24	3.58	4.43	1.73	0.99	4.02
Lu	0.91	0.25	0.44	0.62	0.21	0.12	0.57
ΣREE	223.42	178.09	125.73	122.68	87.87	86.68	309.30
Ta	0.10	0.20	0.20	<0.10	0.10	<0.10	4.90
Hf	0.10	0.40	0.50	<0.10	0.20	0.20	10.00
As	1.90	37.60	133.90	5.10	7.80	7.00	1.50
Ag	<0.10	<0.10	<0.10	<0.10	<0.10	<0.10	<0.10
Au	0.90	1.30	2.10	0.60	2.30	1.00	<0.50
Ga	1.80	1.80	1.80	0.80	2.90	0.60	8.90
Mo	1.30	63.10	18.70	0.20	14.60	8.00	0.60
Cu	0.40	78.30	173.20	3.20	80.20	202.40	1.00
Pb	0.50	1.60	2.00	0.50	1.20	0.50	3.00
Th	<0.2	0.40	0.40	0.40	0.30	<0.2	10.40
U	1.00	1.50	1.30	0.20	1.20	0.70	3.20
Cs	0.10	<0.10	0.10	<0.10	0.30	<0.10	0.40
V	17.00	91.00	72.00	8.00	38.00	8.00	15.00

The C1-chondrite normalized REE of rhabdophane-(Ce) from B46-3 (Fig. 9D) also show strong enrichment in LREE similar to those of synchysite-(Ce).

6. Fluid inclusions

6.1. Petrography

Fluid inclusion analyses were restricted to the two G1 veins in which the rare-earth-bearing minerals occur (see Section 4.1). In the quartz-jasper vein (sample labelled B47) the fluid inclusions occur in quartz together with synchysite, whereas in the quartz vein (B46-3) they occur mainly in the coarse-grained zoned quartz and occasionally in the fine-grained synchysite-bearing quartz. It is important to note that the rare-earth minerals themselves contain no fluid inclusions.

Thick sections from the quartz samples were prepared at the Institute of Mineralogy in Kiel (Germany) with a thickness about 150 μm.

On the basis of their appearances at room temperature, most fluid inclusions are 3-phase liquid-vapour-solid inclusions (LVS inclusions). Although 2-phase inclusions also occur, they were too small to be analysed. The LVS inclusions may even contain two solids and can be considered as complex salt solutions.

The fluid inclusions in both samples show similar characteristics. They are relatively small (generally in the range of 3 to 10 μm, although some can reach 30 μm). The volumes of the phases present in the inclusions were estimated visually. All fluid inclusions are fluid-rich with a liquid phase of about 80 vol%.

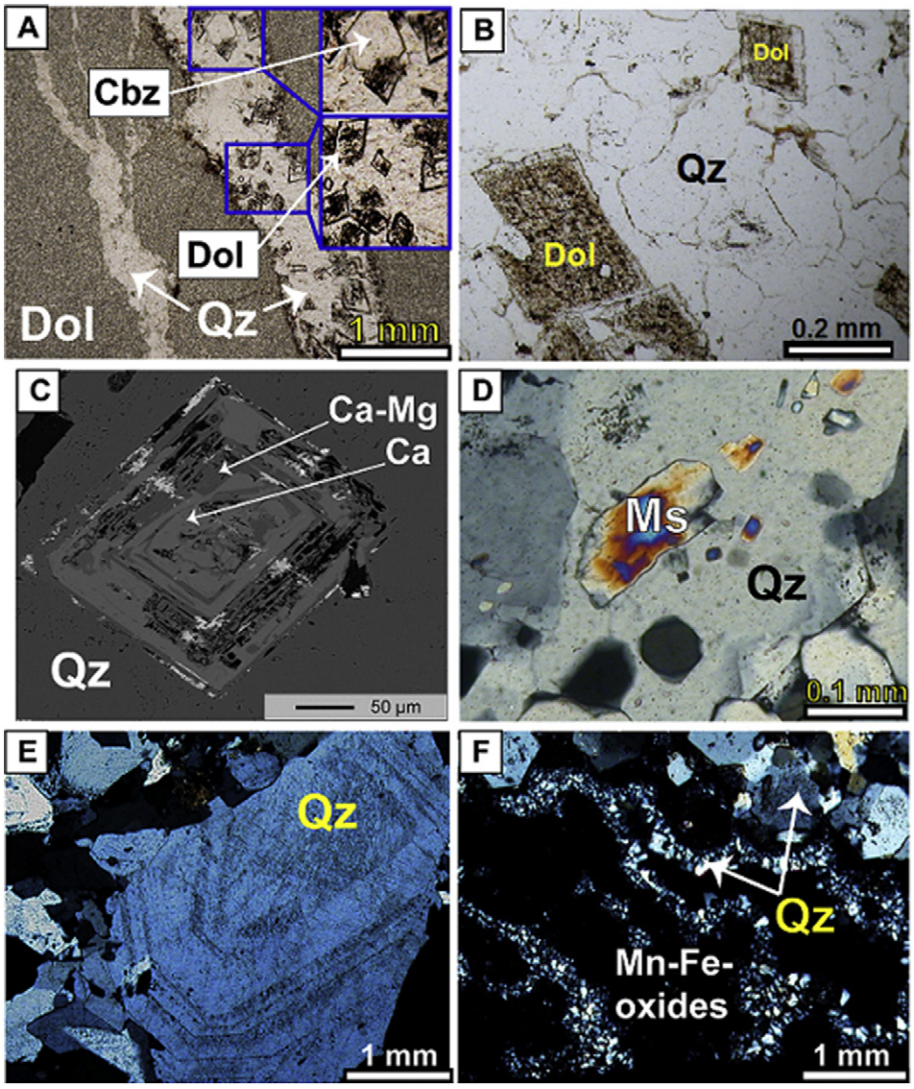

Fig. 7. Sample micrographs: A) dolomite- and chabazite-bearing quartz veins in the lower dolostone. B) Example of idiomorphic carbonate crystals in the quartz veins. C) Back-scattered image of a dolomite rhomb (B) showing zones of Ca and Ca-Mg enrichments. D) Example of muscovite in a quartz vein. E) Zonations of quartz crystals in some quartz veins (B46). F) Crystallization of quartz in the chalcedony form in jasper of quartz-jasper veins (B47).

In the quartz-jasper sample most fluid inclusions occur spatially isolated or in small clusters within the core of the host quartz grains (Fig. 10A, B) suggesting primary formation. Some inclusions in the core have irregular shapes. Fluid inclusions up to 10 μm in size are often subhedral (Fig. 10 C), but some euhedral morphologies are also present (Fig. 10D). Larger elongated and rounded inclusions with sizes up to 30 μm also occasionally occur (Fig. 10E).

Some fluid inclusions show tail-like emanations while still containing fluids and a gas bubble (Fig. 10F) suggesting partial decrepitation.

6.2. Microthermometry

In the REE mineralized quartz-jasper vein most liquid-vapour inclusions homogenize during heating to the liquid phase at temperatures (T_h) between 119° and 256 °C (Fig. 11) with a single exceptions of high homogenization temperatures over 380 °C. In the REE mineralized quartz vein the temperatures of homogenization to liquid phase are between 94° and 260 °C with some exceptions of T_h over 300 °C.

The homogenization temperatures over 300 °C were measured after the measurement of the dissolution temperatures (T_{dis}) for the solid phases. The solid phases in the LVS inclusions in both veins dissolve between 212 °C and 276 °C. These dissolution temperatures would be sufficient to cause decrepitation of fluid inclusions and thus increase the T_h values. That is why all T_h values obtained after the heating up to 276 °C during the measurement of T_{dis} are considered to be unrepresentative homogenization temperatures.

The eutectic temperatures (T_e) are generally between −50° and −54 °C. However during the heating obvious changes in appearance of some fluid inclusions were detected twice at very low temperatures (about −71 °C). These phase transitions at very low temperatures could be a phenomenon of re-crystallization or they could be the result of metastable eutectic temperatures. Solid state transitions are documented for glass in aqueous systems (Angell, 2002). Furthermore final melting temperatures (T_m) of ice in the fluid inclusions of these veins range from 19 °C to 23 °C.

7. Discussion

The main REE mineralized quartz carbonate veins (B46 and B47, Fig 3) only occur north of the syenite pluton, although barren quartz

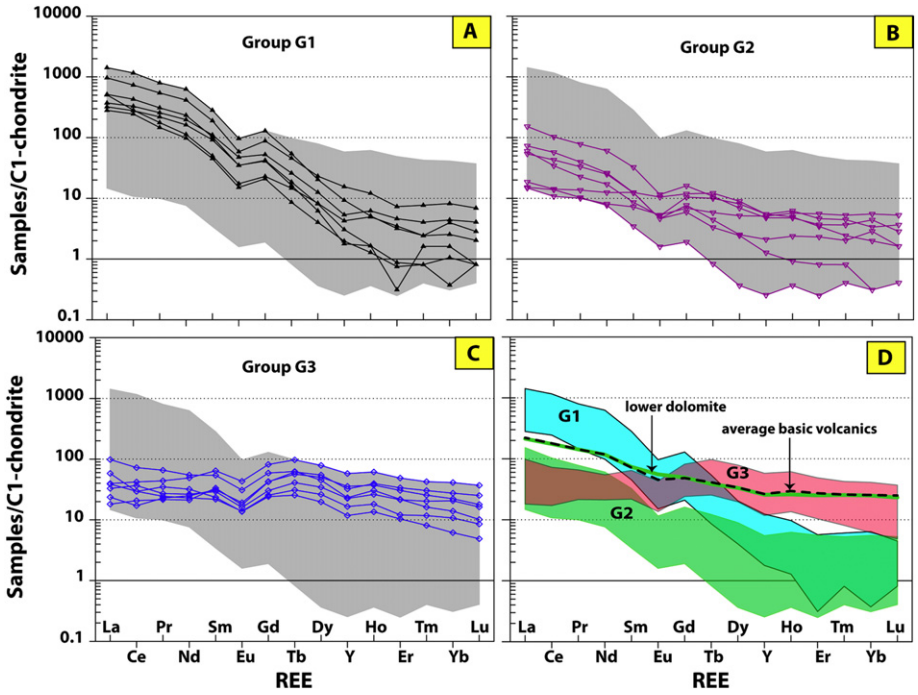

Fig. 8. Chondrite-normalized REE patterns (McDonough and Sun, 1995) of the three vein groups. A) REE spider plot of the REE mineralized veins (G1), B) REE spider plot of the ore-barren veins (G2), C) REE spider plot of the ore-barren veins with flat REE patterns and D) spider plot by group-fields of the three vein groups (G1, G2 and G3). The lower dolostone (B51-1) and the average of the Jbel Boho basic rocks after Benaouda (2015) are added for comparison.

Table 4
Chemical analysis of synchysite-(Ce) in the REE-rich quartz veins (B47 and B46-3). The average 731 values of synchysite in the rhyolitic dyke B35 are from Benaouda (2015).

	Synchysite B46							Synchysite B47						B35
	1	2	3	4	5	6	7	8	9	10	11	12	Average	Average
F	4.36	3.97	4.36	4.52	3.82	4.13	4.20	4.32	4.25	4.36	4.51	4.40	4.27	4.94
CaO	15.56	18.11	18.30	15.74	18.13	18.31	17.79	18.38	18.19	18.07	18.02	18.45	17.75	18.58
La_2O_3	14.46	12.50	12.53	13.23	11.65	12.03	13.16	12.10	12.78	13.21	12.83	13.06	12.79	12.53
Ce_2O_3	22.48	20.70	20.53	21.60	19.85	20.61	21.04	20.06	20.25	19.99	20.68	19.78	20.63	20.35
Pr_2O3	2.75	2.73	2.31	3.02	2.80	2.66	2.38	2.61	2.70	2.63	2.80	2.48	2.66	2.82
Nd_2O_3	10.17	10.23	10.20	10.91	10.85	10.58	9.40	9.62	9.37	9.25	9.75	9.58	9.99	10.60
Sm_2O_3	1.37	1.41	1.30	1.27	1.61	1.56	1.33	1.54	1.21	1.31	1.47	1.13	1.37	1.42
Eu_2O_3	0.11	0.08	0.10	0.10	0.16	0.17	0.00	0.17	0.24	0.18	0.13	0.17	0.13	0.09
Gd_2O_3	0.94	1.04	1.13	1.26	1.40	0.99	0.97	0.99	1.13	0.94	0.94	0.86	1.05	1.03
Dy_2O_3	0.08	0.00	0.00	0.12	0.00	0.00	0.04	0.05	0.04	0.06	0.00	0.07	0.04	0.01
Y_2O_3	0.67	0.43	0.54	0.46	0.35	0.38	0.54	0.74	0.63	0.62	0.54	0.71	0.55	0.39
Er_2O_3	0.00	0.01	0.00	0.02	0.02	0.00	0.00	0.00	0.00	0.00	0.00	0.00	0.00	0.02
Yb_2O_3	0.00	0.00	0.00	0.03	0.00	0.02	0.00	0.07	0.00	0.05	0.03	0.12	0.03	0.01
ThO_2	0.04	0.01	0.01	0.02	0.00	0.00	0.04	0.00	0.00	0.00	0.06	0.02	0.01	0.16
*CO_2	27.02	28.79	28.70	27.71	29.37	28.58	29.36	29.20	29.33	28.25	29.17	28.72	28.72	27.04
SUM	100	100	100	100	100	100	100	100	100	100	100	100	100	100
O ≡ F	1.84	1.67	1.83	1.90	1.61	1.74	1.77	1.82	1.79	1.84	1.90	1.85	1.80	2.08
Total	98.16	98.33	98.17	98.10	98.39	98.26	98.23	98.18	98.21	98.16	98.10	98.15	98.20	97.92
Number of ions based on 7 O														
F	0.77	0.68	0.75	0.78	0.66	0.71	0.72	0.75	0.74	0.76	0.77	0.75	0.74	0.86
Ca	0.93	1.05	1.06	0.92	1.06	1.07	1.04	1.08	1.08	1.06	1.04	1.07	1.04	1.10
La	0.30	0.25	0.25	0.27	0.23	0.24	0.26	0.25	0.26	0.27	0.26	0.26	0.26	0.25
Ce	0.46	0.41	0.41	0.43	0.40	0.41	0.42	0.40	0.41	0.40	0.41	0.39	0.41	0.41
Pr	0.06	0.05	0.05	0.06	0.06	0.05	0.05	0.05	0.05	0.05	0.06	0.05	0.05	0.06
Nd	0.20	0.20	0.20	0.21	0.21	0.21	0.18	0.19	0.19	0.18	0.19	0.18	0.19	0.21
Sm	0.03	0.03	0.02	0.02	0.03	0.03	0.02	0.03	0.02	0.02	0.03	0.02	0.03	0.03
Eu	0.00	0.00	0.00	0.00	0.00	0.00	0.00	0.00	0.00	0.00	0.00	0.00	0.00	0.00
Gd	0.02	0.02	0.02	0.02	0.03	0.02	0.02	0.02	0.02	0.02	0.02	0.02	0.02	0.02
Dy	0.00	0.00	0.00	0.00	0.00	0.00	0.00	0.00	0.00	0.00	0.00	0.00	0.00	0.00
Y	0.02	0.01	0.02	0.01	0.01	0.01	0.02	0.02	0.02	0.02	0.02	0.02	0.02	0.01
Er	0.00	0.00	0.00	0.00	0.00	0.00	0.00	0.00	0.00	0.00	0.00	0.00	0.00	0.00
Yb	0.00	0.00	0.00	0.00	0.00	0.00	0.00	0.00	0.00	0.00	0.00	0.00	0.00	0.00
Th	0.00	0.00	0.00	0.00	0.00	0.00	0.00	0.00	0.00	0.00	0.00	0.00	0.00	0.00
*C	2.05	2.12	2.13	2.07	2.19	2.14	2.16	2.20	2.21	2.20	2.08	2.15	2.14	1.99

* Calculated ΣREE + Th: 0.98; Ca: 1.04; F: 0.74; C: 2.14.

Table 5
Chemical analysis of rhabdophane-(Ce) in the REE-rich quartz vein (B46-3).

Rhabdophane (B46–3)										
	1	2	3	4	5	6	7	8	9	Average
La_2O_3	14.41	14.37	14.49	13.25	15.99	15.25	12.96	15.41	15.27	14.60
Ce_2O_3	31.42	30.17	31.28	25.50	27.70	29.89	26.32	30.88	29.46	29.18
Pr_2O_3	3.35	3.28	3.47	2.71	3.63	3.04	2.79	3.26	3.15	3.19
Nd_2O_3	12.34	12.31	12.29	10.11	13.49	11.67	10.61	11.77	11.44	11.78
Sm_2O_3	1.93	1.87	1.76	1.49	2.06	1.87	1.70	1.63	1.75	1.78
Eu_2O_3	0.19	0.21	0.13	0.00	0.26	0.23	0.05	0.04	0.22	0.15
Gd_2O_3	0.99	1.13	0.86	0.80	1.10	1.09	1.04	0.94	1.17	1.01
Y_2O_3	0.14	0.22	0.14	0.18	0.34	0.31	0.20	0.19	0.34	0.23
ThO_2	0.01	0.05	0.02	0.01	0.01	0.00	0.00	0.00	0.00	0.01
UO_2	0.01	0.05	0.02	0.17	0.00	0.01	0.08	0.02	0.00	0.04
CaO	2.46	2.61	2.28	1.76	2.76	2.94	2.36	2.92	3.71	2.64
P_2O_5	27.61	27.89	27.73	22.58	28.85	27.74	22.63	27.09	27.12	26.58
SiO_2	1.18	1.46	1.70	11.70	0.35	1.11	11.42	0.31	0.31	3.28
Total	96.03	95.61	96.16	90.26	96.54	95.15	92.16	94.45	93.94	94.48
Number of ions based on 4 O										
La	0.21	0.21	0.21	0.17	0.24	0.23	0.16	0.24	0.23	0.21
Ce	0.46	0.44	0.45	0.32	0.41	0.44	0.33	0.47	0.45	0.42
Pr	0.05	0.05	0.05	0.03	0.05	0.04	0.03	0.05	0.05	0.05
Nd	0.18	0.17	0.17	0.12	0.19	0.17	0.13	0.17	0.17	0.16
Sm	0.03	0.03	0.02	0.02	0.03	0.03	0.02	0.02	0.02	0.02
Eu	0.00	0.00	0.00	0.00	0.00	0.00	0.00	0.00	0.00	0.00
Gd	0.01	0.01	0.01	0.01	0.01	0.01	0.01	0.01	0.02	0.01
Y	0.00	0.00	0.00	0.00	0.01	0.01	0.00	0.00	0.01	0.00
Ca	0.11	0.11	0.10	0.06	0.12	0.13	0.09	0.13	0.16	0.11
Th	0.00	0.00	0.00	0.00	0.00	0.00	0.00	0.00	0.00	0.00
U	0.00	0.00	0.00	0.00	0.00	0.00	0.00	0.00	0.00	0.00
P	0.93	0.94	0.93	0.66	0.98	0.94	0.66	0.95	0.95	0.88
Si	0.05	0.06	0.07	0.40	0.01	0.04	0.39	0.01	0.01	0.12
Total	2.036	2.02	2.01	1.80	2.05	2.04	1.83	2.06	2.08	1.99
Calculated formula						REE + Ca				0.99
						P + Si				1.00

carbonate veins are present elsewhere in the Jbel Boho magmatic rocks. The significance of REE transport and deposition in hydrothermal systems depends on several factors e.g. temperature, pressure, pH and the relative concentration of complexing ligands (e.g. F^-, Cl^-, OH^-, SO_4^{2-} and CO_3^{2-}). To understand, why some hydrothermal veins are mineralized while others within the same magmatic complex are not, we discuss in the following sections the hydrothermal conditions for REE transport and precipitation in both the mineralized and the barren veins.

7.1. The REE mineralized veins

Synchysite mineralization occurs in thick hydrothermal veins along a N50°E faulting zone. The fault plane presumably acted as a major fluid pathway, leading to high fluid/rock ratio in comparison to the other veins. This is an important parameter that affects the wall-rock alteration and leads to either significant or negligible mineral deposits.

In the synchysite-bearing quartz-jasper vein (B47), jasper is well consolidated and forms the main volume of the vein. The brown-reddish colour is attributed to Mn-Fe oxide impregnation. The formation of siliceous hydrothermal veins (Jasper, chalcedony) was most likely driven by hydrothermal activity that caused alteration of the host rock. It is cut by a second, younger, generation of quartz veins, which host synchysite mineralization. All minerals were probably deposited from hydrothermal solutions, which also altered the host rock.

The coarse-grained quartz in the synchysite and rhabdophane bearing quartz vein (B46-3) shows anhedral to subhedral crystal shapes and concentric zoning, formed likely during crystal growth within fluid filled cracks (Okamoto and Tsuchiya, 2009). In a manner similar to the jasper-bearing veins, the early-formed, coarse-grained quartz is cut by fine-grained quartz veins, which are associated with synchysite and occasionally rhabdophane. Both REE mineralized veins (B46 and B47) seem therefore to be formed by successive episodes of hydrothermal fluids.

The restricted occurrence of rare rhabdophane-(Ce) in the quartz vein (46-3) indicates limited presence of P in the REE bearing fluid. The high content of Ca and the absence of radioactive elements such as Th in rhabdophane suggests that apatite from the host rock possibly contributed the P to rhabophane in the vein. As both synchysite and rhabdophane have very similar REE composition and co-exist in the same vein, they probably originated from the same hydrothermal fluid.

The dominant salt component in hydrothermal ore fluids is generally the strong electrolyte NaCl, which is most likely the main source of Cl^-. Our fluid inclusion work suggests that the geothermal fluids at Jbel Boho were highly saline. Dissolution temperatures between 210 °C and 280 °C correspond to salinities between 32.4 and 36.7 wt% in a pure halite system (Bodnar, 2003; Bodnar and Vityk, 1994). However, the very low T_e ranging between −50° and −54 °C suggests that NaCl (T_e = 21.2 °C) was not the only salt component of the hydrothermal fluid. Bodnar et al. (2014) and Steele-MacInnis et al. (2011) show experimentally that fluid inclusions from active seafloor hydrothermal systems which show first melting in the vicinity of −50 °C have Ca^{2+} in addition to NaCl.

7.2. Conditions of REE mineralization

Since the discovery of giant REE deposits of hydrothermal origin in China (Bayan Obo), the study of the mobilization of REE in hydrothermal systems has been aimed at understanding why REE are highly mobile in some geological environments.

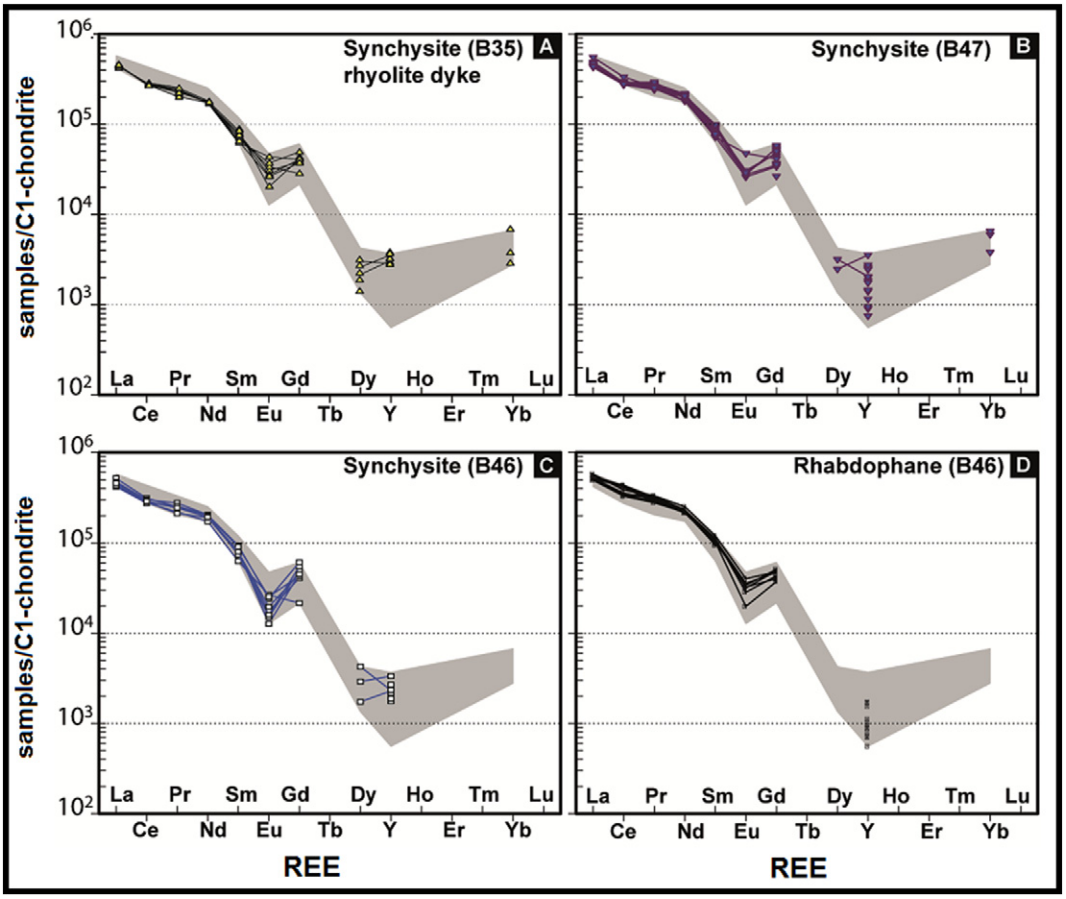

Fig. 9. Chondrite-normalized REE patterns (McDonough and Sun, 1995) of synchysite and rhabdophane from the REE mineralized veins and the late rhyolitic dyke (B35) near the Qz-syenite.

The REE-mineralized and the barren quartz-carbonate veins are hosted in all rock types. Their chemical and mineralogical variations suggest they were formed under a range of conditions with possible variations in: REE concentration in the fluids; temperature; pH; and the availability of the ligands (e.g. Cl^-, F^-, CO_3^{2-}, OH^-) necessary for REE transport and for mineral precipitation. Theoretical estimations and extrapolations of thermodynamic data using Pearson's rules (Haas et al., 1995; Wood, 1990a, 1990b) predicted that the strongest REE complexes would form with F^- and OH^-, moderately weaker complexes with ligands such as CO_3^{2-}, SO_4^{2-}, PO_4^{2-} and HCO^{3-}, and that REE complexes with Cl^- should be the weakest. REE complex stability constants were predicted to increase with increasing temperature (from 25 to 300 °C) at a greater rate for fluoride and carbonate than for other ligands, leading to REE-fluoride complexes being considered as the most favourable candidates for transporting significant REE concentrations in solution and so having the highest ore-forming potential. Based on these theoretical studies and the fact that the REE-F carbonate bastnäsite is the main source of the REE in the world, hydrothermal REE deposits have generally been considered to have been formed by the transport of REE as fluoride complexes (Ruberti et al., 2008; Salvi and Williams-Jones, 1990; Smith and Henderson, 2000; Williams-Jones et al., 2000; Wood and Ricketts, 2000) and high concentration of fluorine in late-stage magmatic fluid were thought necessary to allow REE to be transported in solution (Agangi et al., 2010).

Based on the relative stability of the REE-fluoride and REE-chloride complexes Migdisov and Williams-Jones, (2007) have tested the hypothesis that REE-chloride is unimportant for hydrothermal transport of REE. They demonstrated that high concentrations of chloride complexes can allow comparable transport of REE to that inferred for fluoride complexes at temperatures up to 250 °C. However, this conclusion did not take into account the physicochemical conditions of the fluid or the solubility of the REE-bearing phases.

Recently experimental studies (Migdisov et al., 2009, 2008, 2006, Migdisov and Williams-Jones, 2008, 2007) have shown that these theoretical extrapolations significantly overestimate the stability of REE-fluoride complexes and underestimate the stability of REE-chloride complexes. The cause of these contrasting results is the decrease in the dielectric constant of water with increasing temperature (Williams-Jones et al., 2012). Additionally, REE-fluorides are extremely insoluble over a wide range of pH. Their solubility (and hence the ability of fluoride complexes to transport REE) only increases at relatively low temperature in fluids of intermediate pH conditions which are not expected to occur in most magmatic hydrothermal systems. This implies that, contrary to common assumptions, REE-fluoride species are probably insignificant agent of REE transport in hydrothermal system (Migdisov and Williams-Jones, 2014; Williams-Jones et al., 2012), although F is essential in the precipitation environement to produce REE-F minerals. Instead, REE chloride species dominate and are able to transport appreciable concentrations of REE under acidic conditions.

At Jbel Boho the fluid inclusion studies show that the fluids were highly saline. If these fluids also contained some fluorine in the form of HF, the REE-Ca fluorcarbonate synchysites will precipitate from these saline fluids in response to (a) an increase in pH and (b) a decrease of temperature (Migdisov and Williams-Jones, 2014; Williams-Jones and Migdisov, 2014), both of which reduce the complexing ability of Cl-species. Thin-section observations (Figs. 6 & 7) show considerable quantities of dolomite in the REE mineralized

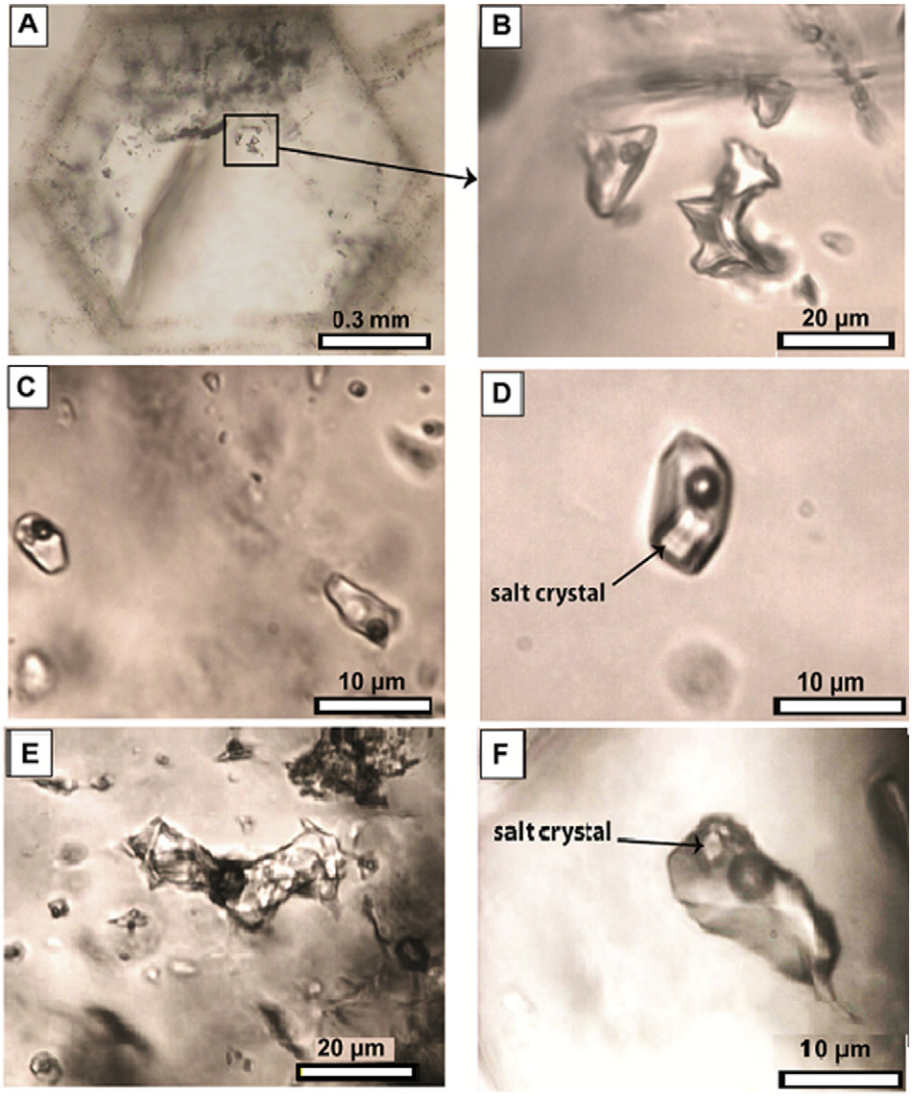

Fig. 10. Photomicrographs (room temperature) of fluid inclusions present in the synchysite-bearing quartz veins. A,B) Fluid inclusions as cluster within a zoned host quartz (B46). C,D) Subhedral to euhedral fluid inclusions (B47). E) Large fluid inclusion surrounded by tiny inclusions (B47). F) Example of partially decrepitated fluid inclusions showing tail form at its end.

veins, a mineral which will dissolve in low-pH environments. This suggests that synchysite precipitation may have occurred due to neutralization of the fluids by either direct contact with carbonate or as the result of mixing of the hot, acidic brines with cooler, high-pH meteoric water that was saturated in carbonate through contact with dolomite. Such interactions will also take place in the presence of abundant Ca^{2+} and HCO^{3-} ions, components which are also necessary to form synchysite. Ngwenya (1994) suggested that a predominance of synchysite over parisite and bastnaesite in REE-mineral assemblages is the result of high $CaCO_3$ saturation.

The formation of synchysite would then occur according to the reaction:

$$REECl^{2+} + HF + Ca^{2+} + 2HCO_3^- = REECa(CO_3)_2F + 3H^+ + Cl^-$$

The presence of fluorine as HF in the saline fluids acts as a binding ligand that promotes REE mineral deposition. The generation of H^+ by this reaction will again decrease the pH, eventually inhibiting synchysite precipitation, making a significant deposition of synchysite only possible where continuous neutralization of the fluid acidity via buffering by carbonate is possible.

e.g. $CaMg(CO_3)_2 + 2H^+ = Ca^{2+} + Mg^{2+} + 2HCO_3^-$

Textural and spatial relationships show no evidence of synchysite crystallization at the expense of pre-existing REE minerals and thus synchysite appears to be precipitated directly from the hydrothermal fluids during neutralization.

Synchysite mineralization was also detected in a late rhyolitic dyke north of the quartz syenite (Benaouda, 2015). Texturally, synchysite is associated with quartz, chlorite and occasionally with Fe-oxides in this dyke. In addition to neutralization of the fluids through interaction with carbonate, hydrothermal alteration of pre-existing Fe-Mg minerals such as hornblende to chlorite is another option to decrease the activity of H^+ and raise pH via the following simplified reaction.

e.g. $Ca_2(Mg, Fe, Al)_6Si_8O_{22}(OH)_2 + 2H^+ + 2H_2O$
$= (Mg, Fe, Al)_6\, Si_4O_{10}(OH)_8 + 4SiO_2 + 2Ca^{2+}$

The similarities of synchysites in both mineralized dyke and veins and their location in the REE mineralized zone north of the quartz syenite indicate that their hydrothermal fluids might have a similar source.

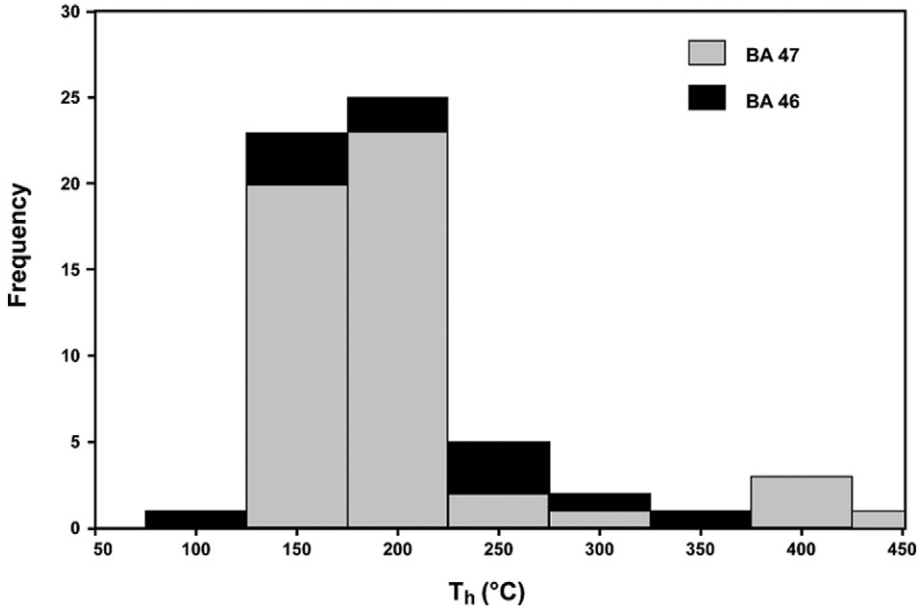

Fig. 11. Histogram of homogenisation temperatures (to the liquid phase) for the studied fluid inclusions in the synchysite-bearing quartz veins (BA 46 and BA 47).

As a source of REE, synchysite has several advantages relative to other minerals. The very high REE contents in the synchysite of Jbel Boho (ca. 50% by mass of the synchysite consists of REE) make it a very concentrated source of REE. Additionally, unlike monazite and allanite, synchysite (and rhabdophane) are very low in both Th and U, thereby reducing complications related to radioactivity during metallurgical processing and making them more ecologically friendly REE-minerals.

The sequence of mineral paragenses for the mineralized veins (B46 and B47) is illustrated in fig. 12. Textural relationships in both mineralized veins clearly show that LREE mineralization only occur in a second

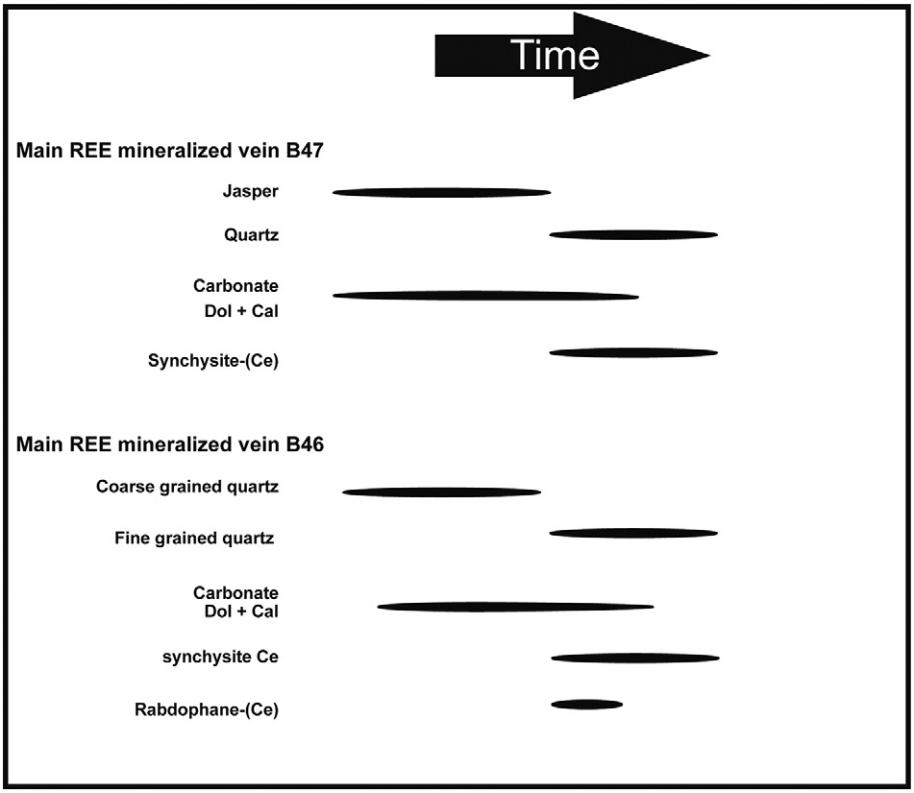

Fig. 12. Proposed paragenetic sequence for the main mineralized veins in Jbel Boho.

hydrothermal phase after either jasper in the vein 47 or the coarse grained quartz in the vein B46 has been precipitated.

7.3. The ore-barren veins

The barren veins (G2, Table 2 and G3, Table 3) occur elsewhere in the Jbel Boho complex and show both different orientations and generally smaller thicknesses (up to 30 cm) than the mineralized veins. Compositionally, the G2 veins overlap with the G1 veins in terms of their HREE contents but have markedly lower LREE enrichment (Fig. 8). The G3 veins overlap with the G2 veins in their LREE contents but have much higher HREE contents, in some cases the HREE contents of the G3 veins are the highest found in the Jbel Boho area.

The REE-composition of the fluid which generated the veins is unknown. However, by analogy with modern-day hydrothermal systems (e.g. Douville et al. (1999) and Craddock et al. (2010)), it is likely to have derived its REE from leaching of the country rock with some fractionation depending on the water/rock alteration reactions occurring and the activity of the available complexing ligands.

Fig. 8D shows the average REE-composition of the basic lavas found at Jbel Boho. The general shape (but not absolute concentrations) of this pattern provides the best information we have on the hydrothermal fluid composition. We note several features:

1. Relative to the lavas, the mineralized G1 veins have steeper REE patterns (Fig. 8A). In particular the very steep Gd-Dy slopes are notable, and mirror well those seen in the individual analyses of synchysite and rhabdophane crystals (cf. Fig. 9).
2. Both the G2 veins and the lower dolostone, which is found intercalated with the basic lava flows, show REE-patterns with very similar slopes to the lavas. This signature in the dolostones is unlikely to be a primary sedimentary feature: REE abundances in sea water range from 10^{-6} to 10^{-4} ppm (Qing and Mountjoy, 1994) and carbonate rocks precipitated from such waters should have very low REE concentrations, even though the partition coefficients of REE between carbonates and saline fluids have been shown to be >100 with minimal fractionation between the REE (e.g. Terakado and Masuda, (1988)). The Jbel Boho lower dolostone, however, also contains tiny quartz-carbonate veins (Fig. 7A), which commonly contain dolomitic rhombs and chabazite, the latter considered to result from alteration of volcanic glass (Mees et al., 2005; Montagna et al., 2010; Weisenberger and Spuergin, 2009). This mineralogy is similar to that seen in the G2 veins, suggesting that the hydrothermal veins dominate the REE signatures in both rock types. Within the veins, it will be the dolomite rhombs, rather than the quartz, which host the REE scavenged from the hydrothermal fluids. The difference in absolute concentrations of REE between G2 and lower dolostones is probably then related to different proportions of vein carbonate in the two rock types.
3. The jasper-bearing veins of group G3 show a different, flatter REE slope associated with high carbonate and iron contents. If deposited from the same fluid as G1, G2 and the lower dolomite veins, then their shallower REE slopes imply that they preferentially either incorporated HREE or did not incorporate LREE from the fluid. The former explanation seems more likely, as $HREE^{3+}$ have ionic radii which are smaller than $LREE^{3+}$ but similar to Fe^{2+} and Mg^{2+} and are known to substitute preferentially for Fe in Fe-oxides. Therefore "mineralogical control" (Bau and Möller, 1992; Morgan and Wandless, 1980) would seem to account for the relative REE abundances in G3 veins.

8. Conclusion

All rock types in the Jbel Boho alkaline igneous complex contain hydrothermal veins showing a distinct texture and mineralogy (usually quartz, carbonate and jasper in variable proportion within the veins).

Several REE mineralized veins contain the REE-F-Ca mineral synchysite and rare REE-P rhabdophane associated with late stage quartz within quartz and jasper veins. The mineralized veins are characterized by very high LREE enrichment and steep middle-REE patterns. The barren veins show either generally low REE contents or high HREE combined with low LREE, probably as result of either limited scavenging of REE from the hydrothermal solution or the presence of Fe-mineral which preferentially scavenge HREE, respectively.

The mineralizing fluid had, based on fluid inclusions, high salinity and probably low pH - transport of REE in solution was as Cl-complexes. Precipitation of REE-containing minerals occurred when this fluid interacted with carbonate (either in HCO_3^- - rich ground water or as dolomites previously present in the veins), raising its pH.

In contrast to other REE-containing minerals such as monazite or allanite, synchysite does not contain appreciable quantities of radioactive elements like U or Th. Together with its high total REE contents, this makes it an interesting REE ore mineral. Late hydrothermal veins associated with alkalic complexes whose environment includes a source of carbonate are good prospection candidates for REE mineralization.

Acknowledgments

Mostafa El Ghorfi, Hassain Baoutoul und Mostapha Amaraki (Managem) provided extensive guidance in the field. Astrid Holzheid und Volker Schenk (Kiel) accompanied part of the fieldwork in 2011. Support of the analytical work by Peter Appel, Barbara Mader and Romain Bousquet (Kiel) is gratefully acknowledged. Andreas Fehler (Kiel) is thanked for the preparation of thin and thick sections. Petra Herms (Kiel) provided extensive help with the fluid inclusion work. We thank the Moroccan mining company Managem for logistical and financial support in the field. Gregor Markl and Michael Marks (Tübingen) are thanked for advice. Michel Jébrak and one anonymous reviewer are thanked for their careful review of our manuscript. This study is part of RB's PhD thesis at the University of Kiel.

References

Agangi, A., Kamenetsky, V.S., McPhie, J., 2010. The role of fluorine in the concentration and transport of lithophile trace elements in felsic magmas: insights from the Gawler Range Volcanics, South Australia. Chem. Geol. 273, 314–325.

Algouti, A., Algouti, A., Chbani, B., Zaim, M., 2001. Sedimentation et volcanisme synsédimentaire de la série de base de l'adoudounien infra-cambrien à travers deux exemples de l'Anti-Atlas du Maroc. J. Afr. Earth Sci. 32, 541–556.

Álvaro, J.J., Ezzouhairi, H., Vennin, E., Ribeiro, M.L., Clausen, S., Charif, A., Ayad, N.A., Moreira, M.E., 2006. The Early-Cambrian Boho volcano of the El Graara massif, Morocco: petrology, geodynamic setting and coeval sedimentation. J. Afr. Earth Sci. 44, 396–410.

Angell, C.A., 2002. Liquid fragility and the glass transition in water and aqueous solutions. Chem. Rev. 102, 2627–2650.

Augé, T., Bailly, L., Wille, G., 2014. An unusual occurrence of synchysite-(Ce) in amygdules from the esterel volcanic rocks, France: implications for rare-earth element mobility. Can. Mineral. 52:837–856. http://dx.doi.org/10.3749/canmin.1400012.

Bau, M., Möller, P., 1992. Rare earth element fractionation in metamorphogenic hydrothermal calcite, magnesite and siderite. Mineral. Petrol. 45:231–246. http://dx.doi.org/10.1007/BF01163114.

Belkabir, A., Jébrak, M., Maacha, L., Samir, M.R.A., Madi, A., 2008. Gold mineralization in the Proterozoic Bleida ophiolite, Anti-Atlas, Morocco. In: Ennih, N., Liegeois, J.-P. (Eds.), The Boundaries of the West African Craton. Vol. 297. Geological Society, London, pp. 249–264 Special Publications.

Benaouda, R., 2015. Magmatic Evolution and REE Mineralization in the Early Cambrian Jbel Boho Complex in the Bou Azzer Inlier (Anti-Atlas/Morocco). (Ph.D. Thesis. Dissertation). Christian-Albrechts Universität, Kiel.

Bodnar, R.J., 2003. Introduction to aqueous-electrolyte fluid inclusions. In: Samson, I., Anderson, A., Marshall, D. (Eds.), Fluid Inclusions: Analysis and Interpretation. Mineral. Assoc. Canada, Short Course 32, Canada, pp. 81–99.

Bodnar, R.J., Lecumberri-Sanchez, P., Moncada, D., Steele-MacInnis, M., 2014. Fluid inclusions in hydrothermal ore deposits. In: Holland, H.D., Turekian, K.K. (Eds.), Treatise on Geochemistry. Elsevier Ltd., Oxford:pp. 119–142 http://dx.doi.org/10.1016/B978-0-08-095975-7.01105-0.

Bodnar, R.J., Vityk, M., 1994. Interpretation of microthermometric data for H_2O-NaCl fluid inclusions. In: De Vivo, B., Frezzotti, M.L. (Eds.), Fluid Inclusions in Minerals: Methods and Applications. Short Course IMA. Virginia Tech, Blacksburg, pp. 117–130.

Broom-Fendley, S., Styles, M.T., Appleton, J.D., Gunn, G., Wall, F., 2016. Evidence for dissolution-reprecipitation of apatite and preferential LREE mobility in carbonatite-

derived late-stage hydrothermal processes. Am. Mineral. 101:596–611. http://dx.doi.org/10.2138/am-2016-5502CCBY.
Choubert, G., 1952. Geologie du Maroc: Histoire geologique du domaine de l'Anti-Atlas. XIXè Congrès Géologique International, Monographies Régionales. Vol. 3, pp. 75–195 Rabat.
Craddock, P.R., Bach, W., Seewald, J.S., Rouxel, O.J., Reeves, E., Tivey, M.K., 2010. Rare earth element abundances in hydrothermal fluids from the Manus Basin, Papua New Guinea: indicators of sub-seafloor hydrothermal processes in back-arc basins. Geochim. Cosmochim. Acta 74:5494–5513. http://dx.doi.org/10.1016/j.gca.2010.07.003.
Dawood, Y.H., Harbi, H.M., Abd El-Naby, H.H., 2010. Genesis of kasolite associated with aplite-pegmatite at Jabal Sayid, Hijaz region, Kingdom of Saudi Arabia. J. Asian Earth Sci. 37:1–9. http://dx.doi.org/10.1016/j.jseaes.2009.05.007.
Donnay, G., Donnay, J.D.H., 1953. The crystallography of bastnaesite, parisite, roentgenite, and synchisite. Am. Mineral. 38, 932–963.
Doroshkevich, A.G., Viladkar, S.G., Ripp, G.S., Burtseva, M.V., 2009. Hydrothermal REE mineralization in the Amba Dongar carbonatite complex, Gujarat, India. Can. Mineral. 47: 1105–1116. http://dx.doi.org/10.3749/canmin.47.5.1105.
Douville, E., Bienvenu, P., Charlou, J.L., Donval, J.P., Fouquet, Y., Appriou, P., Gamo, T., 1999. Yttrium and rare earth elements in fluids from various deep-sea hydrothermal systems. Geochim. Cosmochim. Acta 63:627–643. http://dx.doi.org/10.1016/S0016-7037(99)00024-1.
Ducrot, J., Lancelot, J.R., 1977. Problème de la limite Précambrien-Cambrien: étude radiochronologique par la méthode U-Pb sur zircons du volcan du Jbel Boho (Anti-Atlas marocain). Can. J. Earth Sci. 14, 2771–2777.
El Ghorfi, M., Melcher, F., Oberthür, T., Boukhari, A.E., Maacha, L., Maddi, A., Mhaili, M., 2008. Platinum group minerals in podiform chromitites of the Bou Azzer ophiolite, Anti Atlas, Central Morocco. Mineral. Petrol. 92, 59–80.
Ennaciri, A., Barbanson, L., Touray, J.C., 1995. Mineralized hydrothermal solution cavities in the Co-As Aït Ahmane mine (Bou Azzer, Morocco). Mineral. Deposita 30, 75–77.
Ezzouhairi, H., Ribeiro, M.L., Ait Ayad, N., Moreira, M.E., Charif, A., Ramos, J.M.F., de Oliveira, D.P.S., Coke, C., 2008. The magmatic evolution at the Moroccan outboard of the West African craton between the Late Neoproterozoic and the Early Palaeozoic. In: Ennih, N., Liégeois, J. (Eds.), The Boundaries of the West African Craton. London, Special Publications, Geological Society, pp. 329–343.
Förster, H., 2000. Cerite-(Ce) and thorian synchysite-(Ce) from the Niederbobritzsch granite, Erzgebirge, Germany: implications for the differential mobility of the LREE and Th during alteration. Can. Mineral. 38, 67–79.
Förster, H., 2001. Synchysite-(Ce) solid solutions from Markersbach, Erzgebirge, Germany: REE and Th mobility during high-T alteration of highly fractionated aluminous A-type granites. Mineral. Petrol. 72, 259–280.
Förster, H.J., Ondrejka, M., Uher, P., 2011. Mineralogical responses to subsolidus alteration of granitic rocks by oxidizing As-bearing fluids: REE arsenates and As-rich silicates from the Zinnwald granite, eastern Erzgebirge, Germany. Can. Mineral. 49:913–930. http://dx.doi.org/10.3749/canmin.49.4.913.
Gasquet, D., Ennih, N., Liégeois, J.-P., Soulaimani, A., Michard, A., 2008. The Pan-African belt. In: Michard, A., Saddiqi, O., Chalouan, A., de Lamotte, D.F. (Eds.), Continental Evolution: The Geology of Morocco. Springer, Berlin Heidelberg, pp. 33–64.
Gasquet, D., Levresse, G., Cheilletz, A., Azizi-Samir, M.R., Mouttaqi, A., 2005. Contribution to a geodynamic reconstruction of the Anti-Atlas (Morocco) during Pan-African times with the emphasis on inversion tectonics and metallogenic activity at the Precambrian–Cambrian transition. Precambrian Res. 140, 157–182.
Gieré, R., 1990. Hydrothermal mobility of Ti, Zr and REE: examples from the Bergell and Adamello contact aureoles (Italy). Terra Nova 2, 60–70.
Gieré, R., 1996. Formation of rare earth minerals in hydrothermal systems. In: Jones, A.P., Wall, F., Williams, C.T. (Eds.), Rare Earth Minerals: Chemistry, Origin and Ore Deposits. Chapman and Hall, pp. 105–150.
Guastoni, A., Nestola, F., Giaretta, A., 2009. Mineral chemistry and alteration of rare earth element (REE) carbonates from alkaline pegmatites of Mount Malosa, Malawi. Am. Mineral. 94:1216–1222. http://dx.doi.org/10.2138/am.2009.3185.
Haas, J.R., Shock, E.L., Sassani, D.C., 1995. Rare earth elements in hydrothermal systems: Estimates of standard partial molal thermodynamic properties of aqueous complexes of the rare earth elements at high pressures and temperatures. Geochim. Cosmochim. Acta 59, 4329–4350.
Hikichi, Y., Hukuo, K., Shiokawa, J., 1978. Syntheses of rare earth orthophosphates. Bulletin of the Chemical Society of 51, 3645.
Hikichi, Y., Ota, T., HATTORI, T., Imaeda, T., 1996. Synthesis and thermal reactions of rhabdophane-(Y). Mineral. J. 18, 87–96.
Hikichi, Y., Sasaki, T., Suzuki, S., Murayama, Y., 1988. Thermal reactions of hydrated hexagonal $RPO_4 \cdot nH_2O$ (R = Tb or Dy, n = 0.5 to 1). J. Am. Ceram. Soc. 71, 354–355.
Humphries, M., 2013. Rare earth elements: The global supply chain. CRS Report for Congress 31.
Kijkowska, R., Cholewka, E., Duszak, B., 2003. X-ray diffraction and Ir-absorption characteristics of lanthanide orthophosphates obtained by crystallisation from phosphoric acid solution. J. Mater. Sci. 38, 223–228.
Leblanc, M., 1972. Un complexe ophiolitique dans le Précambrien II de l'Anti-Atlas central (Maroc): description, interprétation et position stratigraphique. Notes et Mémoires du Service geologique du Maroc 236, 119–144.
Leblanc, M., 1981a. Ophiolites précambriennes et gites arseniés de cobalt: Bou Azzer (Maroc). Note et Mémoires du Serveice Géologique (N280, Maroc).
Leblanc, M., 1981b. The late Proterozoic ophiolites of Bou Azzer (Morocco): evidence for Pan-African plate tectonics. Developments in Precambrian Geology 4, 435–451.
Long, K.R., Van Gosen, B.S., Foley, N.K., Cordier, D., 2010. The principal rare earth elements deposits of the United States: a summary of domestic deposits and a global perspective. USGS: Scientific Invistigations Report, pp. 1–14.
Maksimovic, Z., Pantó, G., 1991. Contribution to the geochemistry of the rare earth elements in the karst-bauxite deposits of Yugoslavia and Greece. Geoderma 51: 93–109. http://dx.doi.org/10.1016/0016-7061(91)90067-4.
McDonough, W.F., Sun, S.S., 1995. The composition of the Earth. Chem. Geol. 2541, 223–253.
Mees, F., Stoops, G., Van Ranst, E., Paepe, R., Van Overloop, E., 2005. The nature of zeolite occurrences in deposits of the Olduvai Basin, northern Tanzania. Clay Clay Miner. 53, 659–673.
Migdisov, A.A., Reukov, V.V., Williams-Jones, A.E., 2006. A spectrophotometric study of neodymium(III) complexation in sulfate solutions at elevated temperatures. Geochim. Cosmochim. Acta 70:983–992. http://dx.doi.org/10.1016/j.gca.2005.11.001.
Migdisov, A.A., Williams-Jones, A.E., 2007. An experimental study of the solubility and speciation of neodymium (III) fluoride in F-bearing aqueous solutions. Geochim. Cosmochim. Acta 71:3056–3069. http://dx.doi.org/10.1016/j.gca.2007.04.004.
Migdisov, A.A., Williams-Jones, A.E., 2008. A spectrophotometric study of Nd(III), Sm(III) and Er(III) complexation in sulfate-bearing solutions at elevated temperatures. Geochim. Cosmochim. Acta 72, 5291–5303.
Migdisov, A.A., Williams-Jones, A.E., 2014. Hydrothermal transport and deposition of the rare earth elements by fluorine-bearing aqueous liquids. Mineral. Deposita:1–11 http://dx.doi.org/10.1007/s00126-014-0554-z.
Migdisov, A.A., Williams-Jones, A.E., Normand, C., Wood, S.A., 2008. A spectrophotometric study of samarium (III) speciation in chloride solutions at elevated temperatures. Geochim. Cosmochim. Acta 72, 1611–1625.
Migdisov, A.A., Williams-Jones, A.E., Wagner, T., 2009. An experimental study of the solubility and speciation of the rare earth elements (III) in fluoride- and chloride-bearing aqueous solutions at temperatures up to 300°°C. Geochim. Cosmochim. Acta 73, 7087–7109.
Montagna, G., Bigi, S., Konya, P., Szakall, S., Vezzalini, G., 2010. Chabazite-Mg: a new natural zeolite of the chabazite series. Am. Mineral. 95, 939–945.
Mooney, R.C.L., 1950. X-ray diffraction study of cerous phosphate and related crystals. I. Hexagonal modification. Acta Crystallogr. 3, 337–340.
Morgan, J.W., Wandless, G.A., 1980. Rare earth element distribution in some hydrothermal minerals: evidence for crystallographic control. Geochim. Cosmochim. Acta 44, 973–980.
Nadeau, O., Cayer, A., Pelletier, M., Stevenson, R., Jébrak, M., 2015. The Paleoproterozoic Montviel carbonatite-hosted REE-Nb deposit, Abitibi, Canada: geology, mineralogy, geochemistry and genesis. Ore Geol. Rev. 67:314–335. http://dx.doi.org/10.1016/j.oregeorev.2014.12.017.
Ngwenya, B.T., 1994. Hydrothermal rare earth mineralisation in carbonatites of the Tundulu complex, Malawi: processes at the fluid/rock interface. Geochim. Cosmochim. Acta 58, 2061–2072.
Ni, Y., Hughes, J.M., Mariano, A.N., 1993. The atomic arrangement of bastnasite-(Ce), Ce(C03) F, and structural elements of synchysite-(Ce), rontgenite-(Ce), and parisite-(Ce). Am. Mineral. 78, 415–418.
Oberthür, T., Melcher, F., Henjes-Kunst, F., Gerdes, A., Stein, H., Zimmerman, A., El Ghorfi, M., 2009. Hercynian age of the cobalt-nickel-arsenide-(gold) ores, Bou Azzer, Anti-Atlas, Morocco: Re-Os, Sm-Nd, and U-Pb age determinations. Econ. Geol. 104, 1065–1079.
Okamoto, A., Tsuchiya, N., 2009. Velocity of vertical fluid ascent within vein-forming fractures. Geology 37, 563–566.
ONHYM, 2013. Annual Report 2013. Office National des Hydrocarbures et des mines (ONHYM), Morocco.
ONHYM, 2015. Les Terres Rares Au Maroc. Office National des Hydrocarbures et des mines (ONHYM), Morocco.
Piqué, A., Bouabdelli, M., Soulaimani, A., Youbi, N., Iliani, M., 1999. Les conglomérats du P III (Néoprotérozoïque supérieur) de l'Anti Atlas (Sud du Maroc): molasses panafricaines, ou marqueurs d'un rifting fini-protérozoïque? Comptes Rendus de l'Académie des Sciences-Series IIA-Earth and Planetary Science 328, 409–414.
Qalbi, A., Mouttaqi, A., Rjimati, E.C., Zemmouri, A., Michard, A., Saddiqi, O., 2011. The Nb-Ta-U-REE prospects of the Glibat Lafhouda carbonatites (Awserd Province). Notes et Mémoires du Service geologique du Maroc. 564 (9), 183–187.
Qing, H., Mountjoy, E.W., 1994. Rare earth element geochemistry of dolomites in the Middle Devonian Presqu'ile barrier, Western Canada Sedimentary Basin: implications for fluid-rock ratios during dolomitization. Sedimentology 41, 787–804.
Ridolfi, F., Renzulli, A., Macdonald, R., Upton, B.G.J., 2006. Peralkaline syenite autoliths from Kilombe volcano, Kenya Rift Valley: evidence for subvolcanic interaction with carbonatitic fluids. Lithos 91:373–392. http://dx.doi.org/10.1016/j.lithos.2006.03.026.
Ruberti, E., Enrich, G.E.R., Gomes, C.B., 2008. Hydrothermal REE fluorocarbonate mineralization at Barra do Itapirapua, a multiple stockwork carbonatite, Southern Brazil. Can. Mineral. 46, 901–914.
Salvi, S., Williams-Jones, A.E., 1990. The role of hydrothermal processes in the granite-hosted Zr, Y, REE deposit at Strange Lake, Quebec/Labrador: evidence from fluid inclusions. Geochim. Cosmochim. Acta 54:2403–2418. http://dx.doi.org/10.1016/0016-7037(90)90228-D.
Smith, M.P., Campbell, L.S., Kynicky, J., 2014. A review of the genesis of the world class Bayan Obo Fe–REE–Nb deposits, Inner Mongolia, China: Multistage processes and outstanding questions. Ore Geol. Rev. 1–18.
Smith, M.P., Henderson, P., 2000. Preliminary fluid inclusion constraints on fluid evolution in the Bayan Obo Fe-REE-Nb deposit, Inner Mongolia, China. Econ. Geol. 95, 1371–1388.
Smith, M.P., Henderson, P., Campbell, L.S., 2000. Fractionation of the REE during hydrothermal processes: constraints from the Bayan Obo Fe-REE-Nb deposit, Inner Mongolia, China. Geochim. Cosmochim. Acta 64, 3141–3160.
Smith, M.P., Moore, K., Kavecsánszki, D., Finch, A.A., Kynicky, J., Wall, F., 2016. From mantle to critical zone: a review of large and giant sized deposits of the rare earth elements. Geosci. Front. http://dx.doi.org/10.1016/j.gsf.2015.12.006.

Soulaimani, A., Bouabdelli, M., Piqué, A., 2003. The Upper Neoproterozoic-Lower Cambrian continental extension in the Anti-Atlas (Morocco). Bull. Soc. géol. Fr. 174, 83–92.
Steele-MacInnis, M., Bodnar, R.J., Naden, J., 2011. Numerical model to determine the composition of H_2O-NaCl-$CaCl_2$ fluid inclusions based on microthermometric and microanalytical data. Geochim. Cosmochim. Acta 75:21–40. http://dx.doi.org/10.1016/j.gca.2010.10.002.
Terakado, Y., Masuda, A., 1988. The coprecipitation of rare-earth elements with calcite and aragonite. Chem. Geol. 69, 103–110.
Uher, P., Ondrejka, M., Bačík, P., Broska, I., Konečný, P., 2015. Britholite, monazite, REE carbonates, and calcite: products of hydrothermal alteration of allanite and apatite in A-type granite from Stupně, Western Carpathians, Slovakia. Lithos 236–237:212–225. http://dx.doi.org/10.1016/j.lithos.2015.09.005.
Wang, L., Ni, Y., Hughes, J.M., Bayliss, P., Drexler, J.W., 1994. The atomic arrangement of synchysite-(Ce), CeCaF (CO_3)2. Can. Mineral. 32, 865–871.
Weisenberger, T., Spuergin, S., 2009. Zeolites in alkaline rocks of the Kaiserstuhl Volcanic Complex, SW Germany–new microprobe investigation and the relationship of zeolite mineralogy to the host rock. Geol. Belg. 12, 75–91.
Williams-Jones, A.E., Migdisov, A., 2014. Experimental Constraints on the Transport and Deposition of Metals in Ore-forming Hydrothermal Systems. Vol. 18. Society of Economic Geologists, Inc., pp. 77–95 Special Publication.
Williams-Jones, A.E., Migdisov, A.A., Samson, I.M., 2012. Hydrothermal mobilisation of the rare earth elements - a tale of "Ceria" and "Yttria.". Elements 8, 355–360.
Williams-Jones, A.E., Samson, I.M., Olivo, G.R., 2000. The genesis of hydrothermal fluorite-REE deposits in the Gallinas Mountains, New Mexico. Econ. Geol. 95, 327–342.
Wood, S.A., 1990a. The aqueous geochemistry of the rare-earth elements and yttrium: 2. Theoretical predictions of speciation in hydrothermal solutions to 350 °C at saturation water vapor. Chem. Geol. 88, 99–125.
Wood, S.A., 1990b. The aqueous geochemistry of the rare-earth elements and yttrium: 1. Review of available low-temperature data for inorganic complexes and the inorganic REE speciation of natural waters. Chemical Geology 82, 159–186.
Wood, S.A., Ricketts, A., 2000. Allanite-(Ce) from the Eocene Casto granite, Idaho: response to hydrothermal alteration. Can. Mineral. 38:81–100. http://dx.doi.org/10.2113/gscanmin.38.1.81.
Woolley, A.R., 2001. Alkaline rocks and carbonatites of the world: Africa. Geological Society of London 187–192.
Wu, C., Yuan, Z., Bai, G., 1996. Rare earth deposits in China. In: Jones, A.P., Wall, F., Williams, C.T. (Eds.), Rare Earth Minerals: Chemistry, Origin and Ore Deposits. Chapman and Hall, pp. 281–310.
Zaitsev, A.N., Terry Williams, C., Jeffries, T.E., Strekopytov, S., Moutte, J., Ivashchenkova, O.V., Spratt, J., Petrov, S.V., Wall, F., Seltmann, R., Borozdin, A.P., 2014. Rare earth elements in phoscorites and carbonatites of the Devonian Kola Alkaline Province, Russia: Examples from Kovdor, Khibina, Vuoriyarvi and Turiy Mys complexes. Ore Geol. Rev. 61:204–225. http://dx.doi.org/10.1016/j.oregeorev.2014.02.002.
Zerdane, A., Rjimati, E.C., Zemmouri, A., Mouttaqi, A., Michard, A., 2011. Aghracha iron mine and uranium-REE prospect (Awserd Province). Notes et Mémoires du Service geologique du Maroc 564 (9), 177–182.